Materials Horizons

ROYAL SOCIETY OF CHEMISTRY

REVIEW

View Article Online
View Journal | View Issue

Cite this: *Mater. Horiz.*, 2023, **10**, 3304

Molecularly or atomically precise nanostructures for bio-applications: how far have we come?

Jie Wang, †[a] Ping Li,†[b] Chao Wang,*[a] Ning Liu*[a] and Dongming Xing*[a]

Received 17th April 2023,
Accepted 9th June 2023

DOI: 10.1039/d3mh00574g

rsc.li/materials-horizons

A huge variety of nanostructures are promising for biomedical applications, but only a few have been practically applied. Among the various reasons, the limited structural preciseness is a critical one, as it increases the difficulty in product quality control, accurate dosing, and ensuring the repeatability of material performance. Constructing nanoparticles with molecule-like preciseness is becoming a new research field. In this review, we focus on the artificial nanomaterials that can currently be molecularly or atomically precise, including DNA nanostructures, some metallic nanoclusters, dendrimer nanoparticles and carbon nanostructures, describing their syntheses, bio-applications and limitations, in view of up-to-date studies. A perspective on their potential for clinical translation is also given. This review is expected to provide a particular rationale for the future design of nanomedicines.

Wider impact

Nanostructures with a molecular or atomic structural preciseness distinguish themselves from common nanomaterials. This feature will enable the comparison of material performance across different labs and manufacturers, produce highly repeatable efficacies and predictable side effects, and thereby help to realize the practical bio-application of nanomaterials. It is increasingly recognized that relatively poor structural preciseness is an important reason why the clinical translation of nanomedicines has been outmatched by small molecules and biomacromolecules. Numerous efforts have been devoted to this field, while a precise atomic/molecular arrangement is still difficult to achieve for a nanoparticle containing tens of thousands of atoms, due to the structural complexity and probably the intrinsic limitations in synthesis and characterization techniques. Fortunately, a new dawn has appeared in recent years. Here we summarize the recent advances in this research direction, with a particular emphasis on the advancement in synthesis techniques. Four kinds of nanostructures are at the forefront, each with its own limitations, and insights into the required optimizations for future clinical translation are given.

1. Introduction

Nanotechnology has been flourishing for decades and attracting tremendous efforts to realize its bio-applications. Nanoformulations have been demonstrated preclinically and clinically to possess exceptional advantages over free molecules, including reduced toxicity and improved therapeutic efficiency, but most of the approved or clinically tested drugs are still small molecules or biomarcomolecules. Nano-drugs approved by the Food and Drug Administration (FDA) are mounting, while the majority of them are based on liposomes or the conjugation of polymers.[1] Liposomes are relatively special given the extremely high biocompatibility and the versatile loading pattern for cargos;[2] the conjugation of polymers such as polyethylene glycol (PEG) produces nano-sized formulations but is actually a molecule-based chemical modification method.[3] Natural nanostructures, such as proteins, cell membranes and virus, have achieved great success in clinics and labs, such as the FDA-approved albumin-bound paclitaxel,[4] the extensive exploration of ferritin[5] and cell membrane-derived vesicles[6] as drug carriers, and the use of viral vectors for vaccination, drug delivery and bio-imaging.[7] Nevertheless, employing natural nanostructures may face some challenges including difficulty in large scale production, limited modifiability and potential immunogenicity. Researchers are devoting great efforts to push the clinical translation of the various artificial nanoformulations in the laboratory, which are in much greater variety than those used in clinical settings.

The reasons why nanoformulations cannot match small molecules in clinical translation include a failure to bring improved efficacy or reduced side effects,[8] as well as toxicity-related concerns.[9] Nevertheless, another important reason is being increasingly recognized, which is the lower structural

[a] *The Affiliated Hospital of Qingdao University, Qingdao University, Qingdao 266071, China. E-mail: wangchao20086925@126.com, leirum_ln@qdu.edu.cn, xdm@qdu.edu.cn*

[b] *School of Rehabilitation Sciences and Engineering, University of Health and Rehabilitation Sciences, Qingdao 266071, China*

† These authors contributed equally to this work.

preciseness of nanoformulations compared to small molecules which have defined structures.[10] Nanoformulations that contain multiple ingredients in one particle have been constructed in many studies, raising challenges in practical applications despite the encouraging treatment outcomes; reducing the number of ingredients is helpful, but the particle-to-particle variety of each ingredient is a trickier issue to address.[10] Structure can be highly heterogeneous for a single-component nanomaterial. High structural heterogeneity not only increases batch-to-batch variety but also makes it difficult to study the exact pharmacodynamics and the molecular pathways of drug-body interactions. For example, multiple studies have demonstrated that the drug-to-particle stoichiometry, inter-drug spacing and surface ligand orientation, which are difficult to control for traditional nanostructures, all have a great influence on therapeutic efficiency.[11,12] It is also difficult to compare the efficacy of nanostructures of "one-kind but from different labs", thereby leading to different or even contradictory conclusions. In comparison, molecule-like structural preciseness will facilitate product quality control, yield predictable side effects, enable robust diagnostic and therapeutic performances and realize accurate dosing using a measured amount of product (Fig. 1). In this context, atomically or molecularly precise nanostructures are attracting great interest. Researchers are putting efforts toward fabricating nanomaterials with a defined number and arrangement of atoms/molecules within, by developing new synthesis routes, exploiting the highly specific recognition between chemical (*e.g.*, bonds for click reactions)[13] or biochemical (*e.g.*, nucleic acids, biotin and avidin)[14] entities, *etc.*

DNA nanostructures, some metallic nanoclusters, dendrimer nanoparticles and carbon nanostructures are currently typical nanostructures that can be molecularly or atomically precise. Each has its own way to achieve the high preciseness, and synthetic breakthroughs are the key to success. Therefore, the synthesis routes are fully described in this review. The advantages and limitations of each nanostructure are analyzed with particular attention on the ease of controlling structural preciseness, the facileness for synthesis and the biocompatibility. A perspective on their potential clinical translation is also given. Note that all the introduced are artificial nanostructures, while the biomacromolecule- and cell membrane-based ones are not included since they intrinsically have relatively high structural preciseness and are biomedically promising even regardless of the degree of preciseness.

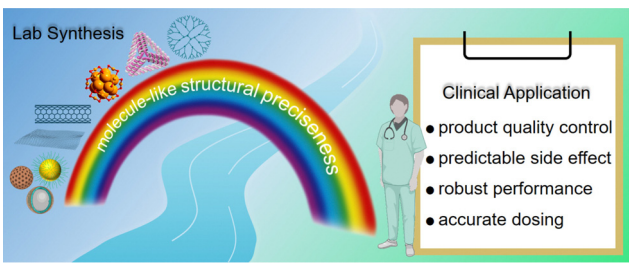

Fig. 1 Illustration of the importance of structural preciseness of nanomaterials for their biomedical applications.

2. DNA nanostructures

2.1. Origin and basic principles

DNA nanotechnology has been explored extensively.[15] As a natural genetic material, DNA follows a strict A–T and G–C pairing law to form Watson–Crick helical double strands that are about 2 nm in diameter and 3.4 nm per helical turn. This provides a highly predictable intermolecular interaction and makes DNA strands natural building blocks for on-demand assembly.[15,16] Seeman *et al.* demonstrated in the early 1980s that by breaking the sequence symmetry of Holliday junctions, one could lock the mobile junction to obtain an immobile structure.[17,18] The immobile Holliday junctions could be considered as a crossover between two DNA duplexes, while stronger junctions such as double crossover,[19] triple crossover,[20] and six-helix bundles[21] have been subsequently constructed by connecting multiple duplexes. By repeatedly assembling these junctions *via* the pairing of cohesive ends, DNA nanostructures will be constructed (Fig. 2a). 3D nanostructures are readily available because the duplexes in the immobile junctions can occupy unparallel planes.[22] This immobile junction-based assembly forms the initial fundamental structure for the synthesis of DNA nanostructures and has inspired various synthesis techniques (Fig. 2). A large variety of DNA nanostructures have emerged with precisely controlled size and structure. Favored by

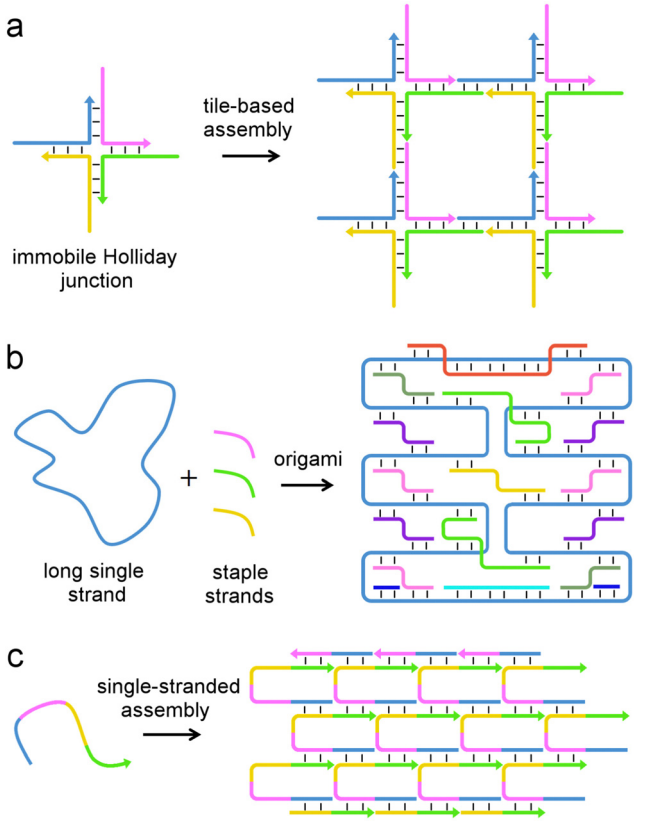

Fig. 2 Typical techniques for DNA nanostructure synthesis. (a) Oligonucleotide tile-based assembly, (b) DNA origami technique, and (c) single-stranded assembly.

the specific recognition between A–T and C–G bases, the inter-particle variation will be limited, probably at a level relevant to the occurrence rate of gene mutation for the simple DNA nanostructures. Moreover, DNA itself can be functional (*e.g.*, therapeutic, diagnostic or recognizable by enzymes) by virtue of a specific nucleotide sequence,[23] which further makes DNA nanostructures biomedically promising.

2.2. Synthesis methods

Seeman's method[22] is a tile-based bottom-up synthesis. Four-arm immobile junctions yield 2D structures, while 3D DNA structures have been built by creating six-arm junctions. For example, Mao *et al.* used a tile-based synthesis for simplified preparation of DNA polyhedra, by using many copies of identical units for hierarchical self-assembly.[24] The formed three-point-star tiles served as vertices to enable the formation of 3D structures; by controlling the flexibility and concentration of the tiles, DNA tetrahedra, dodecahedra and buckyballs were obtained. Tile-based synthesis was the major method during the early years of DNA nanotechnology in virtue of its powerfulness and simplicity.[25,26] Using a number of identical tiles, nanostructures can be obtained after a one-pot annealing treatment. The main drawbacks of this method include the need for high-purity oligonucleotide strands for the formation of tiles, as well as the difficulty in designing the strand sequence.

Nowadays multiple strategies are available, including origami assembly, single-stranded assembly, nanomaterial-templated preparation, *etc.* Origami assembly, which involves the folding of a long single-stranded DNA with the help of short 'staple strands' (Fig. 2b), is a powerful alternative to the tile-based bottom-up synthesis.[29] Its advantages include: (i) the design and synthesis are convenient without the need for sequence optimization and strand purification, and the DNA origami can even be obtained with unpurified staple strands;[15] (ii) the feasibility to obtain uniform products with relatively large size, generally about one order of magnitude larger in size than that obtained from tile-based bottom-up synthesis. Origami assembly readily produces 3D structures, as first demonstrated by Shih *et al.*[30,31] By building staple crossovers to bridge different origami layers, 3D structures formed upon the stacking of the bridged layers, and advanced hierarchical assembly consisting of multiple stacked 3D structures were also obtained.[31] After evolving for more than a decade, DNA origami can now produce nanostructures of almost any topology, including the already reported genie bottle,[31] Möbius strip,[32] spherical or ellipsoidal shells,[33] polyhedral meshes,[27] *etc.* Difficulty in the origami assembly method mainly originates from the need for a large number (generally more than one hundred) of staple strands that will lower the cost-effectiveness, and the total size may be restricted by the length of the long sing-stranded scaffold DNA. Fortunately, computation-aided design and automated routing methods have relieved the difficulty. For example, Högberg *et al.* demonstrated the feasibility of using a routing algorithm and a relaxation simulation to facilitate the synthesis of complex 3D DNA meshes.[27] In the routing algorithm, for a given 3D mesh, the odd-degree vertices were paired and the corresponding edges were assigned as double edges, and then the scaffold was routed based on A-trails (a specific Eulerian trail), followed by the routing of staple strands (Fig. 3a). Computation-aided rotational relaxation and length modification of the arris edges helped to reduce and evenly distribute the strain (Fig. 3b). Very complex structures were designed and successfully synthesized with the help of the routing algorithm and relaxation simulation (Fig. 3c).[27]

A single-stranded assembly method (Fig. 2c), developed in 2012,[37,38] greatly reduces the technological complexity for constructing DNA nanostructures. Yin *et al.* utilized 42-based DNA strands, which were divided into four domains with each acting as sticky ends to bind with four local neighbors, to successfully construct complex 2D patterns.[37] 3D structures were obtained using 32-nucleotide 'bricks' which bind to four local neighbors in a 3D space; each 8-base pair defines a voxel, resembling a Lego-like building block.[38,39] This technique can yield large-sized structures without the limitation of the length of single-stranded DNA in the origami method. Drawbacks of this technique include the increasing number of 'bricks' when preparing larger structures, leading to an increased cost in sequence design; the product yield decreases sharply with the increase of structure size.[15] More recently, Han *et al.* integrated the single-stranded assembly method with the DNA origami technique.[28] By creating a parallel inter-helical cohesion that does not need the strands to cross the central plane (dashed lines in Fig. 3d), knot-free structures were obtained with minimal possibility to be kinetically trapped during the folding process. Moreover, they designed a partially complemented double-stranded DNA (dsDNA), with each paired domain located between two adjacent unpaired domains. Locking domains formed *via* the proximity of two adjacent parallel crossovers after covering one folded layer with another symmetrical layer (Fig. 3e–f).

Since all these strategies applied the basic laws of base-paring and immobile Holliday junction, researchers have integrated different strategies to minimize the disadvantages of each method. For example, Winfree *et al.*[40] and Seeman *et al.*[41] all combined the DNA origami method with tile-based assembly to construct large DNA origami-arrays. All these progresses, along with the wide exploitation of computer-aided sequence design, make DNA nanostructures increasingly easy to prepare.

2.3. DNA nanostructure-based bio-applications

DNA nanostructures possess intrinsic structural preciseness and high biocompatibility, and the on-demand fabricability in sequence, topology and porosity further make them attractive in drug delivery and bio-imaging. Fluorescence,[42] computed tomography (CT),[43] PET[36] and magnetic resonance imaging[44] are all applicable with DNA nanostructures by virtue of the high modifiability of nucleic acid, thereby providing diagnostic information with potential therapeutic value. For drug uploading, drugs can be covalently conjugated, nonspecifically adsorbed (*e.g.*, *via* electrostatic attraction), spatially confined by the porous structure, and the DNA strand itself can be functional *via* sequence design (Fig. 4a). Particularly, doxorubicin (Dox) can

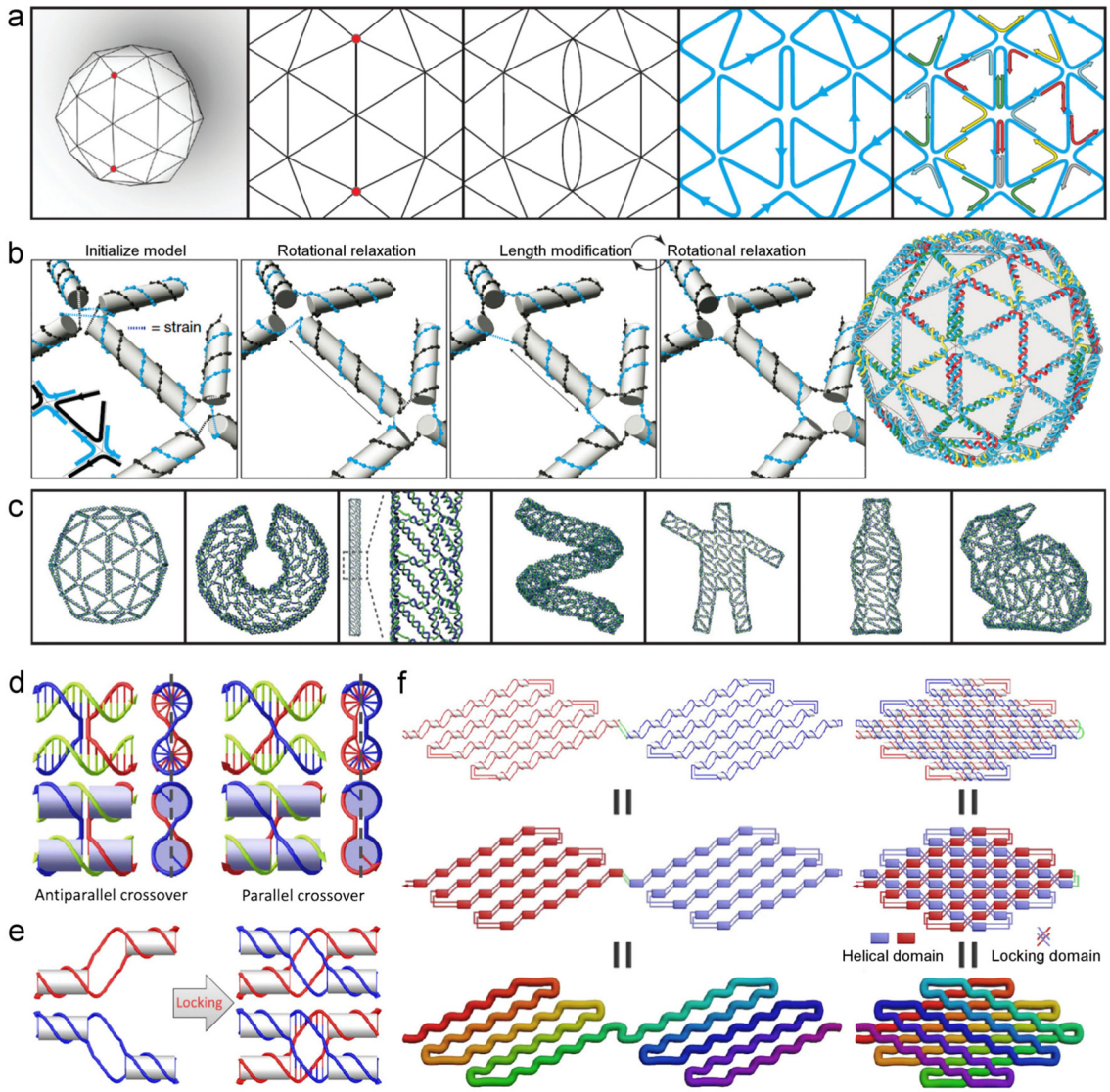

Fig. 3 Typical synthesis strategies for DNA nanostructures. (a and b) DNA origami *via* a routing algorithm. (a) The algorithm process involves drawing a 3D mesh, paring the odd-degree vertices, introducing double edges, routing the scaffold according to A-trails, and then routing the staple strands. (b) Scheme of rotational relaxation and length modification for reducing the strain in the 3D mesh. (c) The multiple complex DNA meshes have been as-designed and prepared. Reproduced with permission.[27] Copyright 2015, Springer Nature. (d–f) Single-stranded assembly. (d) Scheme of the (left) antiparallel and (right) parallel crossover designs. Dashed lines indicate the plane containing all DNA helical axes. (e) Scheme illustrating the formation of a locking domain. (f) Scheme of the formation of single-stranded origami by covering one folded layer with another symmetrical layer. Reproduced with permission.[28] Copyright 2017, American Association for the Advancement of Science.

be stably intercalated into a DNA double helix and will be released at acidic environments due to protonation and the structural metamorphosis of the DNA double helix.[45] For porosity-enabled drug loading, many DNA polyhedra have been used including tetrahedral,[46,47] hexahedral,[48] octahedral,[49] and icosahedral[50] nanocages. Particle morphology is a powerful parameter influencing the delivery efficiency.[51,52] Tetrahedral DNA nanostructures (TDNs) represent the simplest type and are relatively easy and cost-effective to fabricate. They are highly stable against deformable shear force due to the high stability of triangles, and are also proved stable against enzymatic degradation,[53] for example, reported to remain intact in living HEK cells for more than 48 hours.[54] Moreover, TDNs enter cells easily, reported more easily than DNA double strands,[55] which facilitates intracellular drug delivery.

Functionalizing the nucleotide sequence of DNA nanostructures enables stimuli-responsive drug delivery. Gu *et al.* constructed a telomerase-responsive DNA icosahedron by incorporating telomerase primer and telomeric repeats into the icosahedral structure.[56] Platinum nanoparticles were encapsulated as a model drug during the formation of icosahedra, and in the presence of telomerase, the primers were extended, leading to chain substitution and subsequence release of the caged nanoparticles. Douglas *et al.* demonstrated the use of DNA nanobarrels for logic-gated payload release.[57] Each barrel consisted of two domains that were covalently attached in the

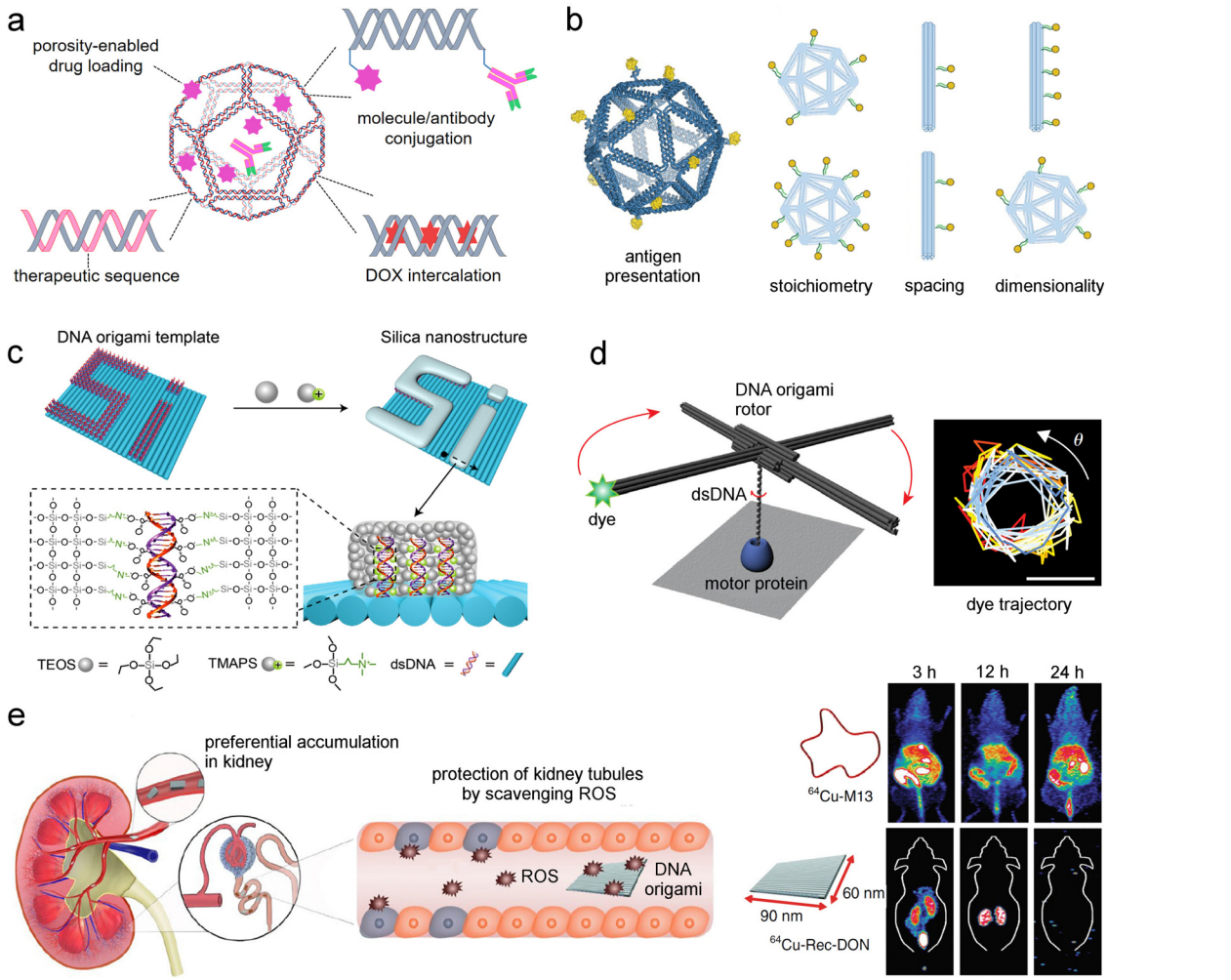

Fig. 4 Bio-applications of DNA nanostructures. (a) Typical drug loading modes of DNA nanostructures. (b) Usage of DNA icosahedra for antigen presentation. Antigen-to-icosahedron stoichiometry, antigen spacing and the dimensionality of carriers were effectively modulated. Reproduced with permission.[11] Copyright 2020, Springer Nature. (c) Scheme of the site-specific synthesis of silica nanostructures on a DNA origami template. Reproduced with permission.[34] Copyright 2018, Wiley-VCH. (d) Scheme of the rotation of dsDNA relative to a surface-bound enzyme, which was amplified using a dye-labelled DNA origami rotor and tracked *via* dye position trajectory. Scale bar: 100 nm. Reproduced with permission.[35] Copyright 2019, Springer Nature. (e) Scheme of the preferential accumulation of DNA origami in kidneys after intravenous injection, and the protection of kidney tubules by scavenging ROS. Positron emission tomography (PET) imaging results of mice injected with either circular single-stranded DNA M13 or rectangular DNA nanostructures, are displayed. Reproduced with permission.[36] Copyright 2018, Springer Nature.

rear and could be noncovalently fastened by staples modified with DNA aptamer-based locks. The locks could be opened by antigen keys *via* switching between an aptamer-complement duplex and an aptamer–target complex. Incorporating two different locks onto the barrel realized an 'AND' logic-gated drug delivery, in which the drug was released only when the two locks were both opened.[57]

The molecular-level preciseness of DNA nanostructures enables many applications that need fine spatiotemporal or stoichiometric control. Bathe *et al.* studied the role of nanoscale antigen organization in B cell activation, where antigens were conjugated onto DNA nanostructures with well-controlled stoichiometry, spacing and dimensionality (Fig. 4b).[11] The results showed that an inter-antigen spacing of ~25–30 nm and the use of a rigid nanostructure were favorable for B cell triggering. Precise synthesis of silica nanostructures were realized by using DNA nanostructures as templates.[34,58] Protruding dsDNA has a stronger affinity to positively charged silica precursors than the DNA origami surface, and therefore silica nanostructures could be precisely prepared *via* the silicification on the designed dsDNA patterns (Fig. 4c).[34] This strategy may pave the way for templated synthesis of a large variety of nanomaterials with DNA nanostructure-like preciseness. Zhuang *et al.* realized the rotation tracking of genome-processing enzymes using DNA origami rotors.[35] dsDNA was attached onto a DNA origami rotor that was labelled with fluorescent dyes, and rotation of the dsDNA relative to a surface-bound DNA-processing enzyme was detected *via* dye position trajectory (Fig. 4d).

In general, DNA nanostructures are promising in multiple bio-applications. Favored by the strict pairing between

complementary nucleotides, the inter-particle variation is quite limited. The number of carried ligands per particle can also be controlled very precisely, which is not easy to achieve using common nanoparticles. This enables precise drug delivery as well as quantitative evaluation about the effect of the delivered agents. Meanwhile, it was suggested by Cai *et al.* that DNA nanostructures (*e.g.*, 2D origamis of around 100 nm in length) exhibited preferential renal uptake and excretion, and alleviated acute kidney injury by scavenging reactive oxygen species (ROS) (Fig. 4e),[36] suggesting a particular application potential in kidney disease treatment. Nevertheless, several shortcomings still exist. First, as a genetic material, DNA is a natural cellular component and has no direct or accurate toxicity, but the long-term biosafety regarding the genetic stability is a potential issue to address.[59] Secondly, large scale (*e.g.*, milligram scale) fabrication of DNA nanostructures is still costly using current techniques, which is not very favorable for wide application. Thirdly, DNA nanostructures may be damaged in nuclease-rich environments. Although not all applications need a high nuclease resistance, this capability will improve the applicability in most scenarios including prolonged circulation in serum.[60] Nevertheless, new techniques are constantly emerging to bring solutions to these issues. For example, the simplification of gene amplification procedures and computer-aided sequence design[61,62] will lower the cost for producing desired nanostructures; strategies of enhancing the nuclease resistance for DNA nanostructures are available, such as using L-DNA[63,64] and increasing the number of DNA crossovers.[65]

3. Atomically precise inorganic nanoclusters

Motivated by the small-size-related properties, synthesizing and applying metallic nanocrystals has been a major research topic in the last two decades. Size and composition are of great significance for their performances in catalysis, bio-sensing and biomedicine. Therefore, reliable preparation that enables precise control over particle characteristics and inter-particle variation is highly desirable. This has been extensively explored at the beginning stage, as an important criterion for optimizing the synthesis procedures. For example, for metal chalcogenide quantum dots (QDs) which have size- and surface-dependent fluorescence,[66] considerable efforts have been devoted to preparing products with highly uniform size/shape and narrow emission width.[67,68] For a nanoparticle of several nanometers in size, it will contain hundreds to thousands of atoms in the particle core and it is difficult to control the exact number of atoms or ligands, although the measured size distribution may be quite narrow. Therefore, as a further step, researchers have been trying to prepare nanoparticles with a defined number of atoms/ligands in the particle core/surface.[69] The spatial arrangement or crystallinity of the atoms is also in atomic precision which finally leads to a well-defined molecule-like chemical structure. This precision is indeed important since the stability and physicochemical properties of nanocrystals are largely a function of the spatial arrangements of atoms (the crystalline phase). Meanwhile, different from common nanoparticles that rely on transmission electron microscopy (TEM) imaging for size determination, these nanoclusters can be characterized with techniques such as single crystal X-ray crystallography (SCXC) and mass spectrometry.[70,71]

3.1. Noble metal nanoclusters

An important type of material in this field is noble metal-based nanoclusters. A pioneering work was reported by Jadzinsky *et al.* who prepared *p*-mercaptobenzoic acid (*p*-MBA)-protected gold (Au) nanoparticles comprised of 102 Au atoms and 44 *p*-MBAs.[72] The central Au atoms were packed in a Marks decahedron and were surrounded by additional layers of Au atoms. SCXC and the electron density map defines an unambiguous particle structure, and it could be confirmed that Au atoms up to 5.5 Å from the particle center did not contact the sulfur on *p*-MBA.[72] Afterwards, dozens of $Au_x(SR)_y$ (SR = thiolate ligand) nanoclusters were reported.[73] The number of Au atoms per particle varies from several to more than one hundred. These materials typically lie in the size regime of smaller than ~3 nm, which enables the Au nanoclusters to exhibit interesting properties different from the common Au nanoparticles (~5–100 nm in size), such as the disappearance of surface plasmon resonance effect and the appearance of the molecule-like HOMO–LUMO electronic transition.[74,75]

For synthesis methods, two main systematic methodologies have been established: the size focusing method[75] and the ligand exchange-induced size/structure transformation (LEIST) method.[76] The size focusing strategy creates a solution environment that makes the $Au_x(SR)_y$ (x and y are exact numbers) particularly stable compared with particles of any other composition. The stable particles are preserved, while the unstable ones reconfigure to be stable; after a required duration (also called aging), highly uniform $Au_x(SR)_y$ are obtained. Jin *et al.* summarized this method as 'survival of the robustest', just like the natural law 'survival of the fittest'.[75] The size focusing process can actually be explained by the potential energy theory which has been applied to guide nanomaterial synthesis,[77] that the given synthesis condition creates a low-energy stable environment for the particles with a 'magic' atom-ligand number and arrangement (Fig. 5). The size focusing method has yielded many $Au_x(SR)_y$,[75] as well as 'common' (without atomic preciseness) nanoparticles with highly uniform size.[78,79] A typical synthesis process involves a preliminary reduction of Au(III) into Au(I) by a thiol-containing ligand in a selected solvent, a further reduction to Au(0) by a strong reductant (*e.g.*, $NaBH_4$) at low temperature, and finally an aging process that allows the size focusing transition to fully occur, during which the reaction can be monitored using techniques such as matrix-assisted laser desorption/ionization time-of-flight (MALDI-TOF) mass spectrometry.[70]

The LEIST method, built on the basis of the size focusing process, involves the transition from one stable size to another. By replacing the original ligands of $Au_x(SR)_y$ *via* ligand exchange, the solution condition becomes unfavorable for the

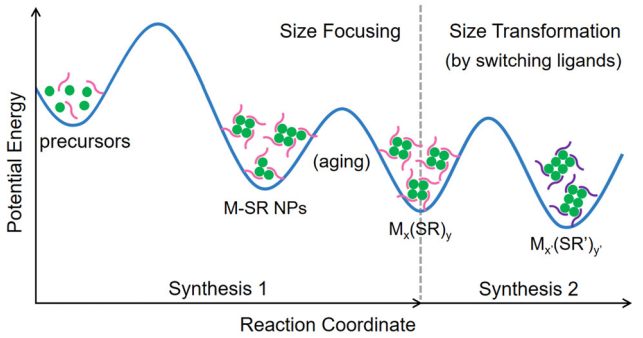

Fig. 5 Illustration of the potential energy of the reaction solution during the synthesis of M-SR NPs, the formation of atomically precise nanoclusters $M_x(SR)_y$ *via* aging, and the formation of new $M_{x'}(SR')_{y'}$ nanoclusters by using new ligands or varying other conditions.

stability of $Au_x(SR)_y$ but creates a new environment that favors the formation of $Au_{x'}(SR')_{y'}$, where the SR′ is the new surface ligand. For example, Wu *et al.* obtained a novel $Au_{60}S_6(SCH_2Ph)_{36}$ nanocluster *via* the LEIST of molecularly pure $Au_{38}(SC_2H_4Ph)_{24}$, where the original and the new ligands only had a subtle difference in structure.[80] Jin *et al.* further showcased the effectiveness of LEIST. Using the isomeric *para*-, *meta*- and *ortho*-methylbenzenethiol (MBT) as surface protecting ligands, Au_{130}(*p*-MBT)$_{50}$, Au_{104}(*m*-MBT)$_{41}$ and Au_{40}(*o*-MBT)$_{24}$ were obtained, respectively.[71] The molecular purity was confirmed by electrospray ionization mass spectrometry (ESI-MS) and MALDI-TOF. Note that replacing original ligands does not guarantee size transformation and only several selected new ligands work for a given synthesis. It has also been confirmed to be feasible to switch ligands of $Au_x(SR)_y$ while keeping the *x* and *y* values constant.[81]

The synthesis of $Ag_x(SR)_y$ follows similar procedures and philosophies with that of $Au_x(SR)_y$. Thiol-containing ligands are usually used due to the ease of Ag–S bond formation.[82,83] Jin *et al.* reported a high yield, large scale preparation method for water-soluble $Ag_7(DMSA)_4$ (DMSA is 2,3-dimercaptosuccinic acid) nanoclusters.[85] The purity was improved *via* post-synthesis precipitation and recrystallization. Other nanoclusters containing Ag atoms ranging from several to dozens have been reported, as summarized in a recent review.[86] It can be noticed that the structure of Ag-based nanoclusters is relatively small (fewer Ag atoms) compared with Au-based ones, making them closer to small molecules. Bakr *et al.* reported a 'golden' $Ag_{25}(SR)_{18}$ nanocluster which shares the identical atom/ligand count, superatom electronic configuration, absorption and emission features, and atomic arrangement, with $Au_{25}(SR)_{18}$.[87] 2,4-dimethylbenzenethiol was used as the SR. Notably, the emission of the $Ag_{25}(SR)_{18}$ reached 850 nm, about 100 nm longer than that of $Au_{25}(SR)_{18}$, representing an advancement in red-shifting fluorescence wavelength. Strategies for enhancing the emission efficiency of Ag nanoclusters have been extensively explored.[88] Generally, Ag-based nanoclusters may have lower biocompatibility compared with Au-based ones,[89] but they are much more cost-effective for large-scale preparation and may achieve wider *in vitro* applications.

3.2. Alloyed nanoclusters and others

Substituting one or more atoms with heteroatom(s) can tune the optical and electronic properties of the original material, forming a strong rationale for the exploration of alloyed nanoclusters. Teo *et al.* pioneered the field by preparing a number of bimetallic (Au–Ag) and trimetallic (*e.g.*, Au–Ag–Pt) nanoclusters.[90,91] Current techniques allow us to precisely control the species, number and position of heteroatoms in one particle, as well as the alloying extent (*e.g.*, bimetallic or trimetallic), therefore providing countless combinations of particle composition (exemplified in Fig. 6). The similar physiochemical properties of Au and Ag drove the emergence of many Au–Ag bimetal nanoclusters. For example, Bakr *et al.* prepared $Ag_{24}Au(SR)_{18}$ nanoclusters *via* a galvanic exchange strategy, using pure $Au_{25}(SR)_{18}$ as the template (SR here is 2,4-dimethylbenzenethiol).[92] The position of the introduced Au was stationary (at the Ag_{25} center). The Galvanic exchange method was proved necessary since the direct preparation of $Ag_{24}Au$ led to mixed products of $Ag_{25-x}Au_x(SR)_{18}$, x = 1–8. More intense alloying, *i.e.*, higher introduced/original atom ratio, can be achieved. Li *et al.* prepared a biicosahedral $[Au_{13}Ag_{12}(PPh_3)_{10}Cl_8]SbF_6$ nanocluster (PPh_3 = triphenylphosphine) by simply reducing the mixture of Au and Ag precursor solutions.[93]

Other metals and metal chalcogenides can also be atomically precise, such as $Cu_{25}H_{22}(PPh_3)_{12}$,[94] $Ni_{39}(SC_2H_4Ph)_{24}$ and $Ni_{41}(SC_2H_4Ph)_{25}$[95] nanoclusters. Pradeep *et al.* reported a Cu_{38}(PET)$_{25}$ (PET here is 2-phenylethanethiol) nanocluster; interestingly, the product exhibited 615 nm photoluminescence which was not common for Cu-based nanoclusters.[96] Owen *et al.* reported multiple atomically precise CdSe QDs, including $Cd_{35}Se_{20}X_{30}L_{30}$, $Cd_{56}Se_{35}X_{42}L_{42}$, and $Cd_{84}Se_{56}X_{56}L_{56}$ (X = O_2CPh, L = H_2N–C_4H_9), whose structures were confirmed

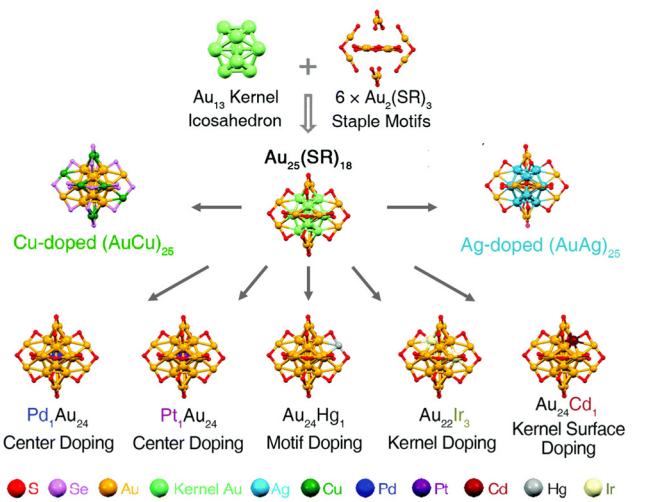

Fig. 6 Feasibility of preparing alloyed nanoclusters *via* doping. Taking $Au_{25}(SR)_{18}$ nanoclusters as an example, Ag-, Cu-, Pd-, Pt-, Cd, Hg- and Ir-doped nanoclusters have been obtained with a controlled number and position of the doping atoms. Redrawn with permission.[84] Copyright 2020, Royal Society of Chemistry.

via single-crystal X-ray diffraction and atomic pair distribution function analysis.[97] Notably, the synthesis route enabled gram scale synthesis and all the nanoclusters were photoluminescent.

3.3. Typical bio-applications

The atomically precise nanoclusters, especially the Au-based ones, have high biocompatibility. Meanwhile, nanoclusters were mostly prepared to be oil-soluble in the earlier studies, while now water-soluble molecules, such as glutathione,[98] captopril[99,100] and *p*-MBA,[72,101] have been increasingly used as capping ligands, thereby paving the way for nanoclusters to be biomedically applied.

As radiocontrast and radiosensitizing agents. Due to the efficient X-ray attenuation, atomically precise Au nanoclusters can be used as radiocontrast agents. Meanwhile, many studies have found their radiosensitizing effect that is helpful for enhancing radiotherapy efficacy. Xie *et al.* reported that ultrasmall $Au_{10-12}(SG)_{10-12}$ (SG = glutathione) nanoclusters exhibited high tumor specificity after being intraperitoneally or intravenously injected, and therefore were a useful contrast agent for CT tumor imaging; the radiotherapy efficacy against U14 tumors in mice was also obviously improved by the nanoclusters.[98] $Au_{29-43}(SG)_{27-37}$ nanoclusters showed similar capabilities.[102] Jia *et al.* reported that Au-levonorgestrel nanoclusters, $Au_8(C_{21}H_{27}O_2)$, could mediate burst ROS generation under X-ray irradiation (Fig. 7a),[103] which might be an origin of the enhancement of radiotherapy. The suppression

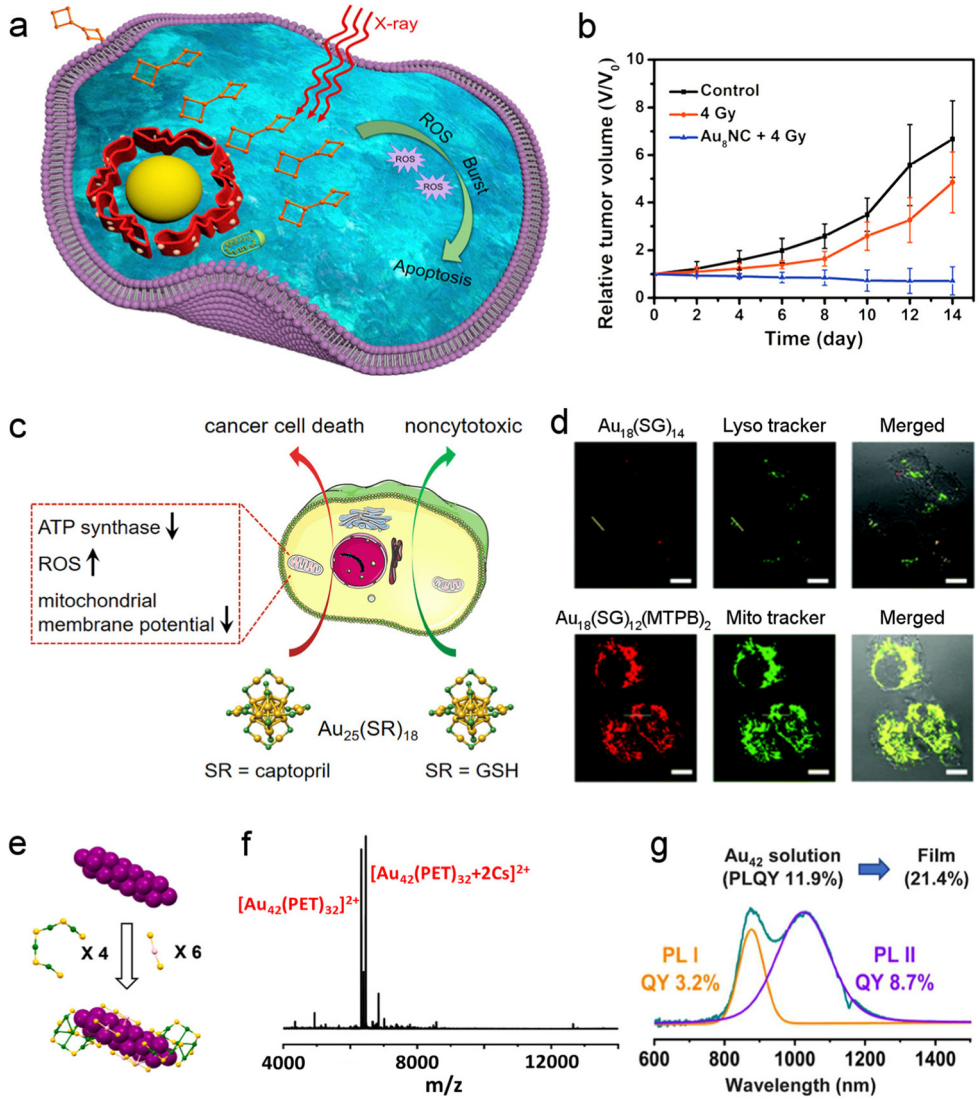

Fig. 7 Multi-roles of nanoclusters in biomedical applications. (a) Schematic illustration of the burst ROS generation of $Au_8(C_{21}H_{27}O_2)$ under X-ray irradiation. (b) Relative tumor volume curves of mice under the indicated treatment. Reproduced with permission.[103] Copyright 2019, American Chemical Society. (c) $Au_{25}(GSH)_{18}$ were nontoxic, while $Au_{25}(Capt)_{18}$ induced cancer cell death by inhibiting ATP synthase, elevating intracellular ROS and disrupting the mitochondrial membrane potential. Reproduced with permission.[100] Copyright 2022, American Chemical Society. (d) Fluorescent $Au_{18}(SG)_{14}$ served as a lysotracker, while $Au_{18}(SG)_{12}(MTPB)_2$ was useful as a mitochondrion tracker. Reproduced with permission.[105] Copyright 2018, Royal Society of Chemistry. (e) Structure of $Au_{42}(PET)_{32}$. Purple: core Au, green: surface Au, yellow: sulfur. (f) Mass spectrum of $Au_{42}(PET)_{32}$. (g) Emission spectrum of $Au_{42}(PET)_{32}$ and the corresponding peak fitting. Reproduced with permission.[106] Copyright 2022, American Chemical Society.

efficiency against EC1 tumors in mice was greatly improved when intraperitoneal $Au_8(C_{21}H_{27}O_2)$ treatment was combined, compared with radiotherapy alone at the same dose (Fig. 7b).

As therapeutic agents and drug carriers. Some nanoclusters can mediate ROS generation under light irradiation and therefore are therapeutic agents *per se*. Jin *et al.* showed that $Au_{25}(SR)_{18}$ (SR = phenylethanethiol or captopril) nanoclusters produced singlet oxygen under light irradiation,[104] which made them applicable in photodynamic cancer therapy by serving as photosensitizers. Meanwhile, nanoclusters are promising drug carriers, when surface-modified with drugs or the ligands themselves are drugs. Compared with common nanoparticles, atomically precise nanoclusters will enable higher drug-to-carrier weight ratio and more precise dosing, due to the ultrahigh specific surface area and the exact number of drugs per particle, respectively; compared with free drugs, those carried by nanoclusters can have lowered toxicity and better efficacy in virtue of the improved pharmacokinetics. Bürgi *et al.* showed that $Au_{25}(GSH)_{18}$ nanoclusters were nontoxic to cells, while $Au_{25}(Capt)_{18}$ nanoclusters induced cancer cell death by inhibiting ATP synthase, elevating ROS levels and disrupting the mitochondrial membrane potential (Fig. 7c).[100] Therefore, nanoclusters are potential drug carriers with much higher delivery efficiency (25 Au atoms deliver 18 captopril in the case above) and more accurate drug loading amount compared with commonly used nanoparticles (*e.g.*, gold or silica nanoparticles).

As fluorescent agents. Many nanoclusters are photoluminescent, thereby having potential in bio-imaging and bio-sensing when the emission efficiency is high enough.[107] Zhu *et al.* summarized the PL tuning methods as engineering of the peripheral ligands, and alloying the pristine metallic structure,[108] just like the philosophy of fluorescent QDs (*e.g.*, CdSe, PbS).[68,88] The capping of surface ligands may be the most influential parameter. For example, Li *et al.* realized the transition of Ag_{20} nanoclusters from non-luminescent to luminescent, *via* ligand replacement.[109] The weakly coordinated NO^{3-} in non-luminescent $Ag_{20}(S^tBu)_{10}(NO_3)_8$ (S^tBu = *tert*-butly thiolate) nanoclusters were substituted by carboxylic ligands, leading to strong green emission. Regarding the alloying strategy, Dolg *et al.* fabricated Ag_{29} and $Ag_{29-x}Au_x$ (x = 1–5) nanoclusters and found that doping with Au atoms significantly enhanced the PL intensity of nanoclusters, especially for the heavily doped ones ($x > 2$).[110] Given these strategies, the PL of nanoclusters has been extensively exploited for bio-imaging. Zhu *et al.* reported a fluorescent nanocluster with a switchable organelle-targeting capability when the surface ligands were switched, so that the $Au_{18}(SG)_{14}$ targeted lysosomes while the $Au_{18}(SG)_{14}(MTPB)_2$ (MTPB = (4-mercaptobutyl)triphenyl-phosphonium bromide) targeted mitochondria (Fig. 7d).[105] Li *et al.* prepared streptavidin- and biotin-modified Au nanoclusters that could assemble on cell membranes *via* antigen-antibody recognition, thereby providing amplified fluorescence signals to lighten cell membranes.[111] Very recently, Luo *et al.* synthesized $Au_{42}(PET)_{32}$ nanoclusters with dual near-infrared (NIR) emissions (Fig. 7e–g).[106] The 875 nm and 1040 nm emission was identified as fluorescence and phosphorescence, respectively. NIR emission has a better tissue-penetration capability than visible light, making these nanoclusters (overall emission quantum yield reached 11.9%) highly promising for *in vivo* bio-imaging.

4. Dendrimer nanoparticles

Dendrimers are nano-sized radially symmetric molecules with well-defined tree-like branches.[112] They are single-polymer nanoparticles, or particulate polymers, that generally have a spherical shape. A dendrimer commonly consists of (i) an initiator core at the center, (ii) multiple branched arms made up of monomers, and (iii) surface functional groups at the end of arms.[113] Each cycle of the radial polymerization is called one generation, and the number of generations is commonly used for describing the size of a dendrimer. The high density in dens, charge or conjugation site makes them promising as drug carriers.[112,114] Here we define dendrimer nanoparticles as either single-molecule dendrimers, supramolecular dendrimers that are assembled from amphiphilic molecules, or nanoparticle-cored dendrimers.

4.1. Dendrimers

Like polymers, the synthesis of dendrimers involves the repetitive conjugation of monomers except that the conjugation occurred radially on the outer surface with self-limited cycles, therefore the structural preciseness of dendrimers should be at the same level as common polymers.[115] The molecule structure cannot expand illimitably, because the number of conjugated monomers will increase exponentially with the increase of generation, while the overall size of the dendrimer does not increase proportionately and cannot provide enough space for further conjugation.[116] As a result, structural defects (missing arms and intramolecular loops) will inevitably occur after a certain number of generations due to the increased steric hindrance. Fortunately, advances in synthetic techniques have helped to effectively overcome or suppress these limitations.

Dendrimer nanoparticles can be synthesized *via* two main routes: divergent synthesis and convergent synthesis. The former is a radial generation-by-generation growth route from the initiator core to outer layers, while the latter needs to prepare multi-generation arms (dendrons) first, followed by coupling the dendrons with the core.[113] The divergent synthesis can yield up to 10 generations or more, however, incomplete reactions occur increasingly. Moreover, the defective impurities produced in divergent synthesis are difficult to separate due to the high structural similarity. Holl *et al.* analyzed 5-generation (G5) poly(amido amine) (PAMAM) dendrimers *via* high performance liquid chromatography (HPLC), mass spectrometry, potentiometric titration, *etc.*[117] Impurities including the generational defects (*e.g.*, those lower than G5) and dimers of G5 could be effectively separated *via* HPLC, and an average of 93 arms could be identified, but the intramolecular branching defects were difficult to directly detect. In the convergent method, dendrons are built separately before the conjugation with the dendrimer core, which provides better control over

defects. Moreover, the impurities generated in convergent synthesis are relatively more different with the desired dendrimers in comparison with those in the divergent synthesis, and thus can be separated more easily.[118] Disadvantages of the convergent method include the reduced reactivity of dendrons with the core due to the increased steric hindrance. Notably, the divergent and convergent methods are not mutually exclusive, since a number of studies have combined the two strategies to achieve better quality control. This combined strategy involves the synthesis of a low-generation dendrimer as the supercore and low-generation dendrons as arms, which are then coupled to produce the final dendrimer.[119] Higher generations can be realized *via* this approach.

Structural purity will be guaranteed when every reaction step proceeds with high yield. ''Click'' chemistry has been used to prepare dendrimers due to their high reaction specificity and yield.[120] For example, Wong *et al.* reported an efficient approach to prepare glycerol dendrimers *via* thiol-yne click chemistry.[121] *Via* a simple divergent route, G3 dendrimers were obtained without transition metal catalysis or heating, and the structural purity was suggested by nuclear magnetic resonance (NMR) results, mass spectrometry as well as gel permeation chromatography.

4.2. Supramolecular dendrimers

To obtain higher generation dendrimers or simplify the synthesis procedures, researchers developed dendrimer-mimics consisting of amphiphilic dendrons, which usually bear a hydrophobic tail and multiple hydrophilic arms.[122,123] The amphiphilic dendrons would self-assemble into supramolecules in an aqueous environment *via* noncovalent interactions. This strategy is a simplified convergent method that has removed the difficulty in conjugating the large dendrons onto the core, and makes the supramolecule resemble micelle or liposome which has achieved wide clinical applications.[2] Therefore, the structural preciseness of these supramolecular dendrimers should be comparable to liposomes, with reduced structural defects compared with the same-generation single-molecule dendrimers. Peng *et al.* fabricated supramolecular dendrimers *via* the self-assembly of low-generation PAMAM dendrons, and the products exhibited a highly narrow size distribution.[123] Using click chemistry to prepare the amphiphilic dendrons will further improve structural preciseness.[124]

4.3. Nanoparticle-cored dendrimers

Nanoparticle-cored dendrimers are another category of dendrimer nanoparticles that use nanoparticles as cores for the conjugation of dendrons.[126] Researchers have fabricated these dendrimers to deliver the core nanoparticle, make the dendrimers multifunctional, or to create a large number of anchoring sites for the ease of conjugation by dendrons. The high hydrophilicity of the chosen dendrons can also water-solubilize the hydrophobic nanoparticles. Nanoparticle-cored dendrimers can be prepared *via* replacement of original ligands by dendrons, post-synthesis conjugation of dendrons onto nanoparticles, or directly using dendrons as protecting ligands during nanoparticle synthesis.[127] Obviously, the structural preciseness of nanoparticle-cored dendrimers largely depends on the used nanoparticles; using materials/molecules with well-defined structures as the core will improve the preciseness. For example, Zhou *et al.* fabricated molecularly precise cyanine nanodots, by using cyanine dyes as cores to prepare polylysine dendrimers (Fig. 8a–b).[125] MALDI-TOF, gel permeation chromatography and HPLC demonstrated the product purity, and the nanodots were shown to be applicable for *in vitro* and *in vivo* bio-imaging (Fig. 8c).

4.4. Preclinical applications

Advances in synthetic techniques led to the emergence of various dendrimers including PAMAM,[118] poly(arylether),[128] polylysine,[129] triazine[130] and phosphorus dendrimer.[131] The polycationic nature of PAMAM, polylysine and phosphorus dendrimers makes them suitable for gene delivery.[132] Shi *et al.* used phosphorus dendrimers as a nonviral vector to deliver plasmid DNA.[133] Interestingly, it was found that G1 dendrimers displayed a higher delivery efficiency to HeLa cells compared with G2 and G3 counterparts, suggesting a critical role of the particle size. Self-assembled supramolecular dendrimers were also widely used. Peng *et al.* reported a dual-targeting dendrimer-mediated siRNA delivery system for cancer therapy.[134] Amphiphilic PAMAM dendrimers self-assembled into micelle-like structures and efficiently adsorbed siRNA, while a RGDK peptide (which could bind integrin and neuropilin-1 receptor on cancer cells) was further decorated onto the micelle surface to achieve tumor-specific siRNA delivery. The system was further demonstrated to be useful for tumor PET imaging when modified with ^{69}Ga (Fig. 8d–f).[123] Compared with [^{18}F]FDG (^{18}F labelled 2-fluorodeoxyglucose, the clinical gold reference for PET imaging), the dendrimer-based agent showed a better detection capability for multiple cancers including colorectal cancer and pancreatic cancer (Fig. 8g), possibly due to the higher intratumoral accumulation of nanoparticles compared with small molecules.

Toxicity is a critical issue determining the application potential. It has been summarized that the cytotoxicity of dendrimers mainly depends on the generation, as well as the number and nature (anionic, neutral or cationic) of the terminal moieties,[135] and therefore precise control of the particle structure is needed to improve *in vivo* biocompatibility. High-generation cationic dendrimers are relatively cytotoxic compared with the low-generation ones. Wang *et al.* reported generation-, concentration- and time-dependent hemolysis of PAMAM dendrimers when incubated with red blood cells.[136] The hemolysis effect followed G6-NH_2 > G5-NH_2 > G4-NH_2 > G3-NH_2, and the surface modified PAMAM-COOH and PAMAM-OH dendrimers induced much less hemolysis. Mukherjee *et al.* found previously that the short-term and long-term cytotoxicity of PAMAM dendrimers to both HaCaT and SW480 cells followed G6 > G5 > G4.[137] A mechanism study revealed that dendrimers would be located in the mitochondria and lead to ROS production, apoptosis and DNA damage.[138] Surface modification with negatively charged or neutral groups decreased

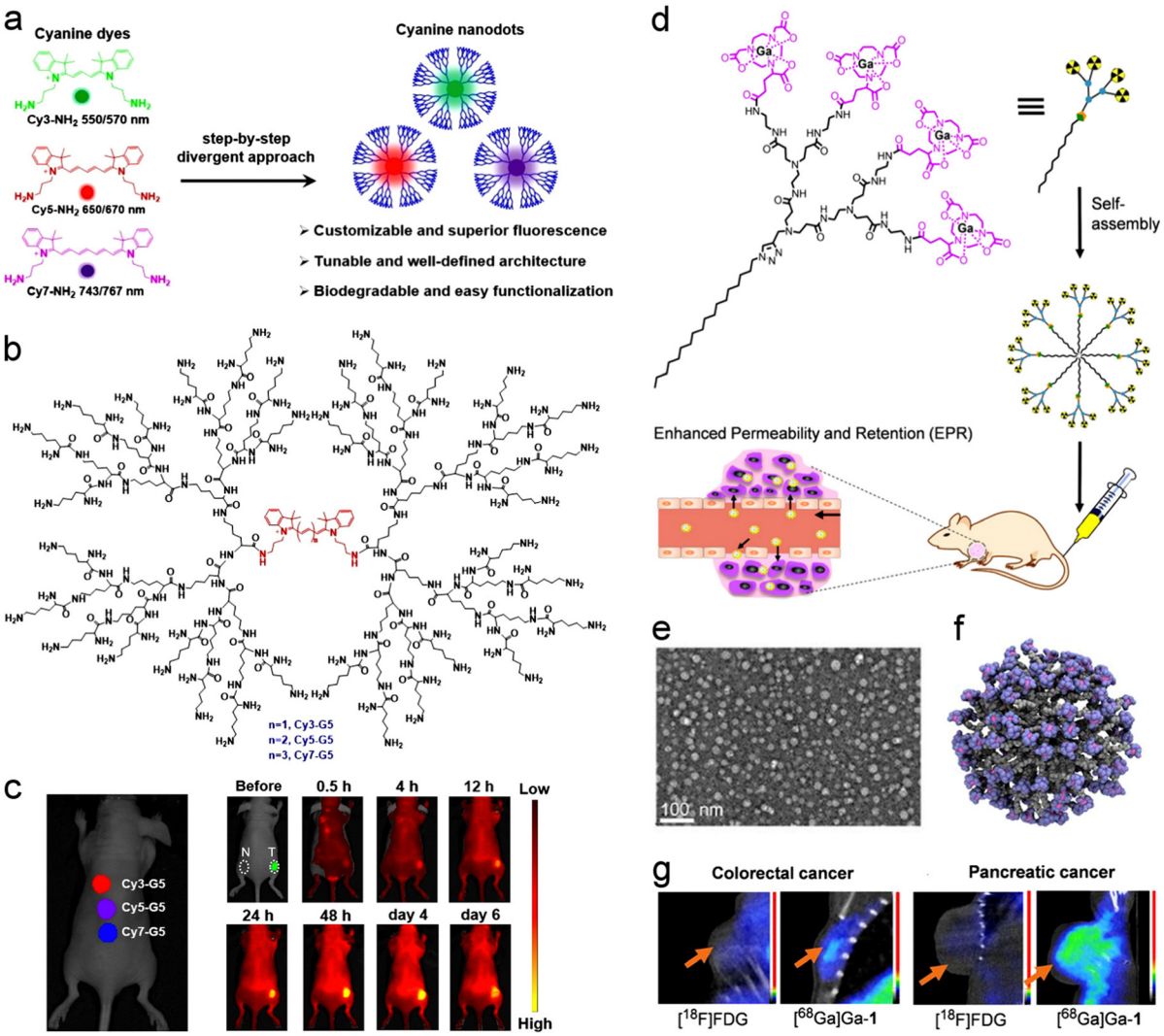

Fig. 8 Biomedical applications of dendrimer nanoparticles. (a) Representation and some merits of cyanine-cored dendrimers. (b) Chemical structure of the cyanine-cored dendrimers. (c) Usage of cyanine-cored dendrimers for *in vivo* mice imaging. Reproduced with permission.[125] Copyright 2022, Wiley-VCH. (d) Schematic illustration of a supramolecular dendrimer nanosystem, based on the self-assembling of ^{69}Ga-labelled amphiphilic dendrimer, for mice PET imaging. (e) TEM image and (f) molecular-dynamics simulation model of the supramolecular dendrimers. (g) PET imaging of colorectal and pancreatic tumors on mice injected with [^{18}F]FDG or ^{69}Ga-labelled supramolecular dendrimers. Reproduced with permission.[123] Copyright 2018, National Academy of Science.

cytotoxicity.[139] Siegwart *et al.* used an alternative method to reduce toxicity by fabricating degradable dendrimers.[140] Ester linkage was used to link the dendrimer core with the arms, and hepatotoxicity assays as well as liver cancer treatment outcomes suggested a balanced low toxicity and high treatment potency.

4.5. Clinical trials

There are multiple ongoing clinical trials involving the use of dendrimers, as summarized in Table 1. A majority of the ongoing trials, including several completed ones (not listed in Table 1), were launched by the Ashvattha Therapeutics, Inc., which focuses on the development of a new class of precision medicines using hydroxyl dendrimers. The hydroxyl dendrimers are used as drug carriers to minimize toxicity and maximize drug uptake in the disease tissue.[141] About four dendrimer-based formulations have been developed by the company and tested in clinical trials, but it is difficult to identify their exact structures. After injection or oral dosing, the dendrimers distribute rapidly throughout the body, and the water-like surface makes them behave comparably to water without binding proteins. Enabled by their unique surface chemistry and small size, the developed dendrimers can travel across the blood–brain barrier. Moreover, they can be taken up selectively by disease cells including inflammatory cells, and as a carrier are excretable through the kidney without causing systemic toxicity. The completed trials (*e.g.*, NCT04321980 and NCT03500627) have suggested the safety and high tolerability of the hydroxyl dendrimers. Surface conjugation with ^{18}F makes the dendrimers a potential contrast agent.

Table 1 Ongoing dendrimer-involved clinical trials

Dendrimer	Indication	Trial purpose	Start date	Identifier and phase
^{18}F hydroxyl dendrimer	Amyotrophic lateral sclerosis	Study the PK, safety and distribution of the dendrimer as an imaging agent	July 2022[a]	NCT05395624; Phase 1
NAC-conjugated G4 PAMAM[146]	Severe COVID-19	Study the efficacy and effect in reducing pro-inflammatory cytokines in severe COVID-19	August 2020	NCT04458298; Phase 2
Hydroxyl dendrimer	NVAMD; DME	Study its safety, tolerability and PK in patients with NVAMD or DME	August 2022	NCT05387837; Phase 2
Hydroxyl dendrimer	NVAMD; DME	Study its safety, tolerability and pharmacokinetics in healthy volunteers	January 2022	NCT05105607; Phase 1
^{188}Re ligand-loaded G5 poly-L-lysine[142]	Primary or metastatic liver cancer	Study its efficacy and safety in treating non-responding and inoperable liver cancers	March 2017	NCT03255343; unknown
PEGylated poly-L-lysine dendrimer	Non-Hodgkin lymphoma	Study the safety, tolerability, PK and preliminary efficacy of the dendrimer in patients with NHL	July 2022	NCT05205161; Phase 1 and 2

PK: pharmacokinetics; NAC: *N*-acetyl-cysteine; NVAMD: neovascular age-related macular degeneration; DME: diabetic macular edema. [a] Estimated start date.

^{188}Re reagent (^{188}Re-nitro-imidazole-methyl-1,2,3-triazol-methyl-di-(2-pycolyl)amine)-loaded G5 poly-L-lysine dendrimer, also known as "[^{188}Re]rhenium-ImDendrim" (Fig. 9), co-developed by French and Chinese researchers, is being tested as a potential radiopharmaceutical. Its anti-tumor activity has been confirmed in a liver cancer model in nude mice.[142] Positive outcomes after intrahepatic injection to a human patient with adenocarcinoma and liver metastases have also been reported.[143] More recently, [^{188}Re]rhenium-ImDendrim has been trailed to treat patients with local primary and secondary lung malignancies *via* brachytherapy (NCT03255343).[144]

Generally, we noticed that all the trialed dendrimers were single-molecule dendrimers rather than self-assembled dendrimer supramolecules or nanoparticle-cored dendrimers. This may be due to three main reasons: (i) The development of dendrimer-based nanomedicines is still at the early stage, as all the relevant trials were launched in the last five years. (ii) Single-molecule dendrimers are more suitable for some scenarios. For example, they are generally smaller than antibodies or antibody fragments, which is important for urinary excretion and crossing tissue barriers,[145] while supramolecular dendrimers will be too large to achieve the same. (iii) Inter-particle structural variation of supramolecular and nanoparticle-cored dendrimers may challenge the quality-control and the precise evaluation of pharmacokinetics and therapeutic efficacy. Nevertheless, supramolecular dendrimers possess their own advantages for bio-applications, such as higher drug loading capacity. Wider applications of dendrimers can be expected under constant efforts to improve synthetic techniques. Meanwhile, all the trialed formulations are administrated *via* intravenous injection, while localized delivery is also a powerful route worthy of exploration.[147]

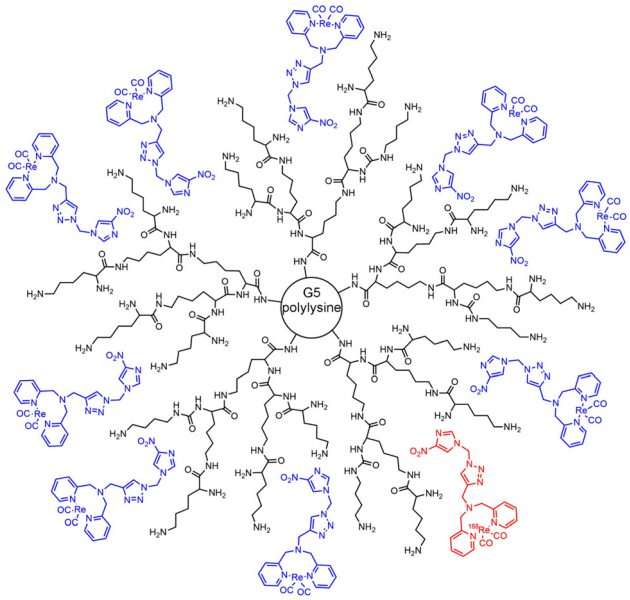

Fig. 9 Chemical structure of the [^{188}Re]rhenium-ImDendrim.

5. Carbon nanostructures

Carbon nanostructures, including fullerene, carbon nanotubes, graphene nanosheets and nanoribbons, have been widely studied due to their high biocompatibility, eco-friendliness, unique optical and electronic properties and high stability.[148] They can be regarded as an intermediate between small molecules and nanomaterials, and between inorganic and organic materials. Fullerene is a structurally precise molecule, while for other carbon nanostructures the synthesis techniques have been extensively evolved to enable the preparation of structurally highly uniform products.[149]

5.1. Graphene nanosheets and nanoribbons

Graphene is a single-layered graphite material with zero bandgap, and when its lateral size decreases to the nanoscale, it becomes a graphene nanosheet (GNS) with a size-dependent bandgap. GNSs have exceptional properties such as the large edge effect and ultra-high specific surface area, and one particular merit of GNSs compared with other carbon nanostructures is the ease of exhibiting photoluminescence. A quantum yield of greater than 50% has been reported;[150] for tuning PL emission wavelength, several strategies were demonstrated to be effective, such as enlarging the sp^2 domain by conjugating

GNSs with extra aromatic rings, and introducing an intermediate n-orbital between π and π* orbitals *via* conjugation with electron-donating groups.[151,152] Meanwhile, GNSs are considerably biocompatible, and have been reported to be less toxic compared with microscale graphene.[153]

GNSs can be prepared using the techniques commonly used for nanomaterial synthesis, including the top-down route by cutting, exfoliating or grinding bulk materials, and the bottom-up route by building nanostructures from atoms and molecules *via* hydrothermal/solvothermal treatment, microwave treatment, or traditional organic chemistry.[154–157] The bottom-up route is more effective in quality control and property modulation.[158] For example, incorporating heteroatoms into the basal plane of GNSs is easier through bottom-up routes compared with the top-down routes. It is currently hard to achieve high control over product quality through a simple and large-scale synthesis route (*e.g.*, one-step hydrothermal treatment) without a separation procedure. Song *et al.* achieved space-confined formation of GNSs by hydrothermally treating citrate which was intercalated into the interlayer galleries of layered double hydroxides.[159] The obtained GNSs had a highly narrow size distribution and was basically all single-layered due to the strict space-confinement. An aromatic $C_{27}H_{10}N_2O_{15}$ molecular structure was revealed by ^{13}C NMR, ^{1}H NMR, gel permeation chromatography and tandem mass spectrometry.[159] This method produced much more uniform GNSs compared with the common one-step hydrothermal syntheses, but still failed in providing atomic preciseness.

Given the well-defined structure of hexagonal carbon arrangement,[160,161] GNSs hold the possibility to be precisely prepared *via* the traditional organic synthesis route. Organic synthesis can guarantee the high structural preciseness *via* stepwise monitoring and purification, and has been demonstrated to be feasible for GNS synthesis.[149] For example, Yan *et al.* reported the synthesis of colloidal GNSs through the oxidative condensation of polyphenylene dendritic precursors, yielding graphene moieties of up to 170 carbon atoms.[162] The graphene was stabilized by multiple 2′,4′,6′-triakyl phenyl groups that were covalently attached to graphene edges. Nitrogen-doping and addition of functional groups were shown to be feasible to tune the bandgap and optical property of the resulting GNSs.[163,164] These products represent the most uniform kind of GNSs despite the tedious synthesis procedure and the failure in providing detectable photoluminescence and being water-solubilized.

Graphene nanoribbons (GNRs) are a member of the graphene family but different from common graphene nanosheets. They have a narrow width (typically several nanometers) and large aspect ratio, resemble a linear polymer and therefore have reduced dimensionality compared with graphene sheets.[167] Their remarkable mechanical, thermal, electrical and optical properties offer many opportunities in bio-applications.[168] The structural variation for a GNR mainly comes from the varied length and edge structure. Top-down routes, for example cutting graphene *via* lithography, generate products with relatively low uniformity,[169] while some established bottom-up routes have produced atomically precise GNRs. Ruffieux *et al.* prepared atomically precise GNRs *via* surface-catalyzed coupling of molecular precursors into linear polyphenylenes and subsequent cyclodehydrogenation.[170] By using different monomers, the topology, width and edge periphery were effectively modulated. Raman spectroscopy and scanning tunneling microscopy demonstrated the atomic preciseness of straight, chevron-type and threefold junction GNRs. Crommie *et al.* further prepared atomically precise GNR heterojunctions. Fluorenone GNRs were first synthesized by annealing a molecule precursor on the Au(111) surface, and chevron GNRs were then obtained following post-growth excitation (Fig. 10a). Formation of fluorenone/pristine chevron heterojunctions was confirmed *via* multiple techniques including bond-resolved scanning tunneling microscopy (Fig. 10b).

An important issue restricting the bio-applications of these atomically precise GNRs is the limited water-solubility. Graphene oxide nanoribbons, in which the carbon atoms are partially sp^3-hybridized by bearing oxygen-containing functional groups, may be more applicable due to their higher water-solubility and ease of functionalization.[171] Nevertheless, the introduction of oxygen-containing groups inevitably decreases the structural preciseness since the extent and position of oxidation are difficult to control.

5.2. Carbon nanotubes

Carbon nanotubes (CNTs) are cylindrical molecules that are composed of rolled-up single-layer carbon atoms (graphene). Since the first discovery in the early 1990s,[172] numerous studies have explored their synthesis, property and application. The diameter of CNTs is typically measured in nanometers, while the length can reach millimeters. CNTs are mostly prepared *via* chemical vapor deposition, which involves the splitting of a carbon-containing precursor gas (*e.g.*, CO, methane) to deposit carbon atoms on catalyst nanoparticles (*e.g.*, Fe, Co) to generate CNTs.[173] Visually uniform products have been produced in good controllability and scalability, but atomic preciseness is barely achieved. The floating catalyst chemical vapor deposition, featured by the *in situ* formation of catalyst nanoparticles, is to some extent helpful to improve structural preciseness,[176] but it raises another problem, *i.e.*, the collected CNTs will be attached with a large number of catalyst nanoparticles.[177] Generally, the diameter of CTNs prepared *via* this route is relevant with the size of the catalyst nanoparticles which are heterogeneous, while CTNs with close diameters are hard to separate. Meanwhile, multiple-walled CTNs may be simultaneously generated, and structural defects on the wall plane may emerge.[178] Other synthesis methods including arc discharge and laser ablation are also bothered by these limitations. Fortunately, integrating organic synthesis with the surface-catalyzed carbon atom deposition method is applicable to greatly improve the structural preciseness.

By vertically 'stacking' carbon atoms on some already-existing carbon nanorings (*e.g.*, cycloparaphenylenes, cyclacene), we can obtain open-ended CTNs with a tuned structure: the CTN diameter could be tuned by selecting differently sized carbon nanorings, while the use of chiral carbon nanorings led to chiral CTNs.[179] For example, Itami *et al.* prepared

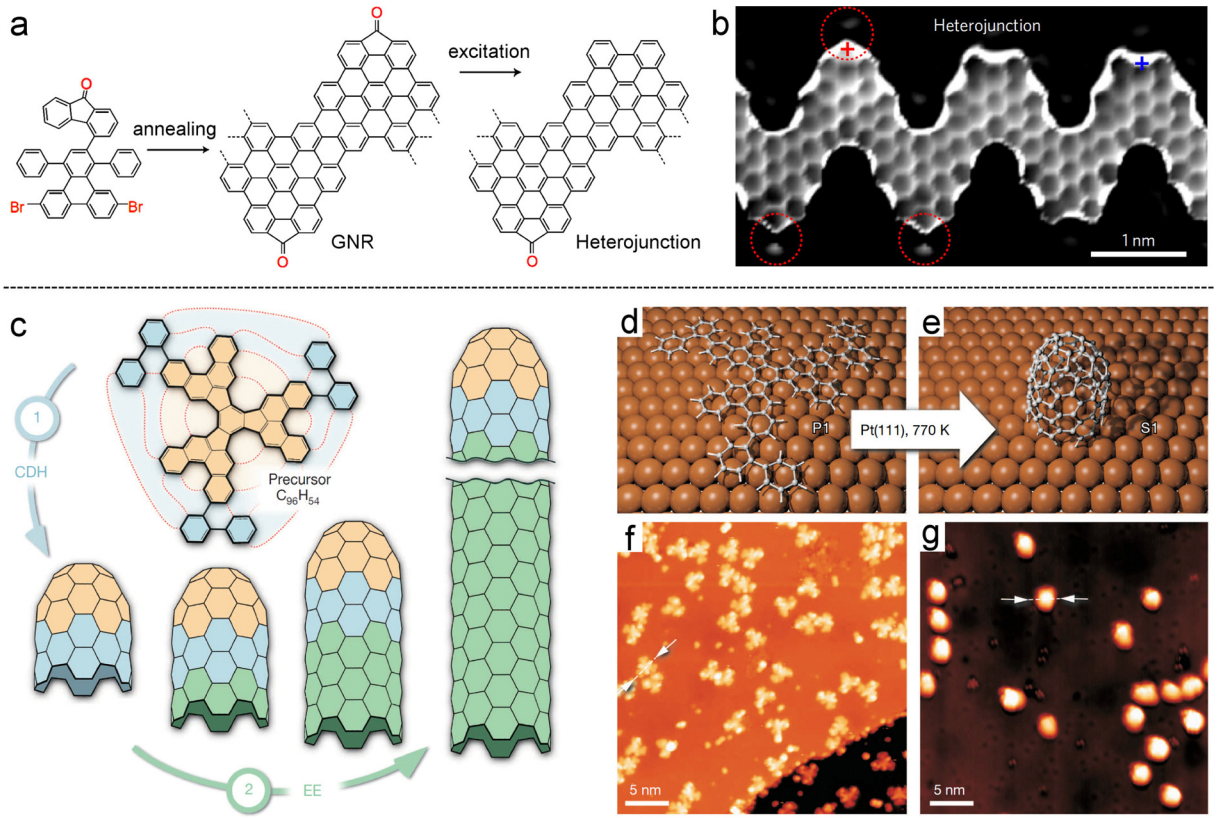

Fig. 10 Atomically precise carbon nanostructures. (a) Synthesis route of an atomically precise GNR and the corresponding heterojunction. (b) Bond-resolved scanning tunneling microscopy image of the fluorenone/pristine chevron heterojunction. Reproduced with permission.[165] Copyright 2017, Springer Nature. (c) Synthesis route of singly-capped CNTs using a cap-molecule (precursor $C_{96}H_{54}$). Illustration of the conversion of (d) cap-molecule to (e) the ultrashort singly capped CNT seed *via* thermal induced surface catalyzed cyclodehydrogenation. The corresponding scanning tunneling microscopy images of (f) cap-molecules and (g) CNT seeds on the Pt(111) surface. Reproduced with permission.[166] Copyright 2014, Springer Nature.

structurally uniform CTNs by simply heating cycloparaphenylenes (as templates) with ethanol (as the carbon source), realizing a 'growth-from-template' route.[180] Cycloparaphenylenes with the number of phenylenes from 9 to 16 were used to effectively tune the CTN diameter. The same group also prepared a chiral carbon nanoring, cyclo[13]paraphenylene-2,6-naphthylene, which represented a novel chiral template.[181] Using cycloparaphenylenes as templates leads to 'armchair' edges, while using cyclacene will yield 'zigzag' edges, although the synthesis of cyclacene has virtually not been realized.[149] Meanwhile, besides open-ended CTNs, capped CTNs can be prepared by selecting some capping molecules as templates. Fasel *et al.* achieved controlled synthesis of singly-capped CTNs by first synthesizing an elaborately designed cap-molecule and then converting the cap-molecule into an ultrashort singly capped nanotube seed, followed by nanotube growth *via* epitaxial elongation (Fig. 10c–g).[166] The cap-molecule was deposited onto a Pt(111) surface and then annealed to induce cyclodehydrogenation reaction to form the singly caped seed, and epitaxial elongation was achieved by incorporating carbon atoms decomposed from ethylene or ethanol.

Generally, organic synthesis of template molecules greatly improves the structural preciseness of CTNs, especially in the control of the diameter, chirality and edge structure. Nevertheless, it is technically difficult to realize full synthesis using organic chemistry, and surface-catalyzed carbon deposition at a high temperature is needed to construct the main body of CTNs. Consequently, strict atomic preciseness is difficult to achieve. What might relieve this limitation is that in bio-applications such as drug delivery, a relatively short length is needed for CTNs, which will decrease the reaction duration of surface catalyzed carbon deposition and therefore decrease the structural variation. Moreover, using large carbon nanorings (*e.g.*, cycloparaphenylene and cyclacene) as templates will make it easier to yield a large diameter, which is desirable for the uploading of biomacromolecules.

5.3. Carbon quantum dots

Carbon quantum dots (CQDs) are zero-dimensional quasi-spherical carbon nanomaterials. Synthesis of CQDs is facile, usually *via* solvothermal treatment of small molecules or biomasses. The precursors in the high temperature and high pressure environment will undergo some 'miraculous' reactions that are not be easy to realize *via* common organic synthesis, leading to the formation of crystalline structures that are often fluorescent.[182] It is currently very difficult to prepare atomically precise CQDs, despite the fine control of synthesis procedures and the use of simple molecular precursors.

Given the ultra-small size, researchers are binding synthesis optimization with purification techniques such as liquid chromatography to improve the product uniformity. Emission width has been widely employed to assess the size uniformity of CQDs.[183] Yang *et al.* prepared triangular CQDs with unprecedented narrow emission bandwidth.[174] Using phloroglucinol as the precursor, highly luminescent CQDs were obtained after solvothermal treatment in ethanol at 200 °C, and the products was further purified *via* silica column chromatography. The high color purity made the CQDs comparable with traditional dyes in providing non-overlapping multicolor fluorescence signals (Fig. 11a–d).[174] Generally, the structural preciseness of CQDs may be at a similar level as other common nanomaterials such as CdSe QDs and gold nanoparticles.

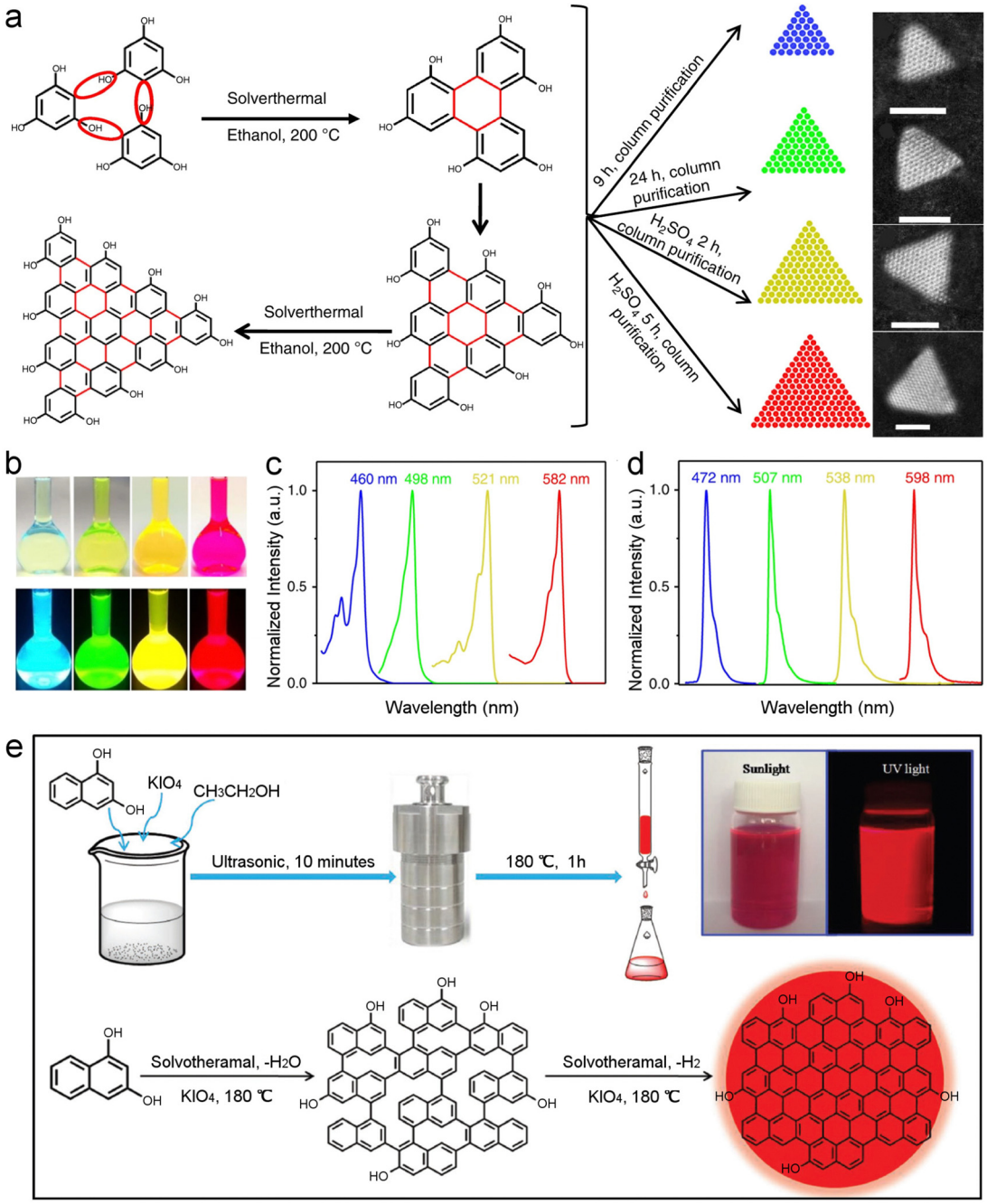

Fig. 11 Structurally uniform CQDs. (a) Synthesis route of triangular CQDs *via* solvothermal treatment of phloroglucinol, and the dark-field scanning transmission electron microscopy images of differently sized triangular CQDs. Scale bar, 2 nm. (b) Photographs of the solutions of blue-, green-, yellow- and red-emissive CQDs under daylight and UV light. (c) Normalized absorption spectra and (d) normalized PL spectra of the corresponding CQDs. Reproduced with permission.[174] Copyright 2018, Springer Nature. (e) Synthesis route and growth mechanism of the 53% efficient red emissive CQDs. Reproduced with permission.[175] Copyright 2017, Wiley-VCH.

Emission efficiency of CQDs has been improved to a level comparable to organic dyes, such as those prepared by solvothermally treating 1,3-dihydroxynaphthalene and KIO_4 (Fig. 11e).[175] The CDs had a quantum yield of 53% at a red emission wavelength, thereby showing great potential in *in vivo* bio-imaging. Still, column chromatography was needed to improve the product purity.

6. Perspective remarks and conclusion

Molecule-like structural preciseness is a large challenge for nanomaterials on the way towards practical bio-applications, as it ensures product quality control and repeatable interaction with the human body. The efforts devoted to synthesis method exploration have yielded great uniformity in size, composition and surface chemistry, as often confirmed by microscopic observation, hydrodynamic diameter measurement, or the consistency and uniformity in properties. Nevertheless, greater preciseness is expected for bio-applications and the typical characterization methods for nanomaterials may not guarantee a molecule-level preciseness (Fig. 12). For example, for crystalline nanostructures that are characterized to be highly uniform, the particle size and shape may be variable; the number, position and species of lattice defects will greatly differ among particles; the location and conformation (protruding or prostrating) of surface ligands are difficult to identify under common characterizations. Particle size, shape and lattice defects determine the electronic and optical performances, while the density and orientation of ligands have a great impact on *in vivo* particle behaviors such as the affinity toward the cell surface and circulation time in blood.

Therefore, molecule-like structural preciseness may be difficult to realize *via* regular synthesis-characterization-optimization cycles. Sharp evolvement in synthesis strategies will be needed. DNA nanostructures, atomically precise nanoclusters, dendrimer nanoparticles and carbon nanostructures are currently representative materials that can reach molecule-like preciseness, and each has its own way to ensure a highly precise structure, and each has its own potential in specific bio-applications. For example, dendrimer nanoparticles are promising in both drug delivery and bio-imaging after the required modification, as evidenced by multiple clinical trials; the potential of Au-based nanoclusters in fluorescence imaging may be less pronounced due to the relatively low emission efficiency, but a particular promise is held in CT imaging due to the low toxicity and high X-ray attenuation efficiency of Au. Nevertheless, practical bio-applications are currently rarely realized, suggesting the need for further progress in synthesis methods and property optimization.

(i) DNA nanostructures are composed of molecularly precise nucleic acids that are organized by the strict pairing law between complementary bases, and therefore can achieve high structural preciseness despite the relatively sophisticated structure. Synthesis methods have evolved to be increasingly facile and robust, including the computation-aided sequence design[61] and the non-necessity of staple strands in the newly-developed single-stranded assembly method.[39] Nevertheless, for advanced 3D structures it is still hard for the structural uniformity to reach a similar level as that for simple structures such as DNA tetrahedra and small 2D structures. Meanwhile, two other limitations are restricting the wide application of DNA nanostructures, which are the high cost for large scale production, and the long-term biosafety regarding generic stability.

(ii) The atomically precise $M_x(SR)_y$ nanoclusters are prepared *via* reduction of metal precursors in the presence of surface ligands, followed by an aging process during which the particle size focuses. Pure MS spectra and the feasibility for SCXC measurement suggest the high structural preciseness. The nanoclusters are promising as imaging contrast agents. Meanwhile, the SR-to-M ratio is defined for a species, meaning that the drug (SR) content is constant for a specific weight of particles, which is essential for accurate dosing. The SR-to-M ratio in nanoclusters is also much higher compared with that in nanoparticles of larger size, since the particle volume increases

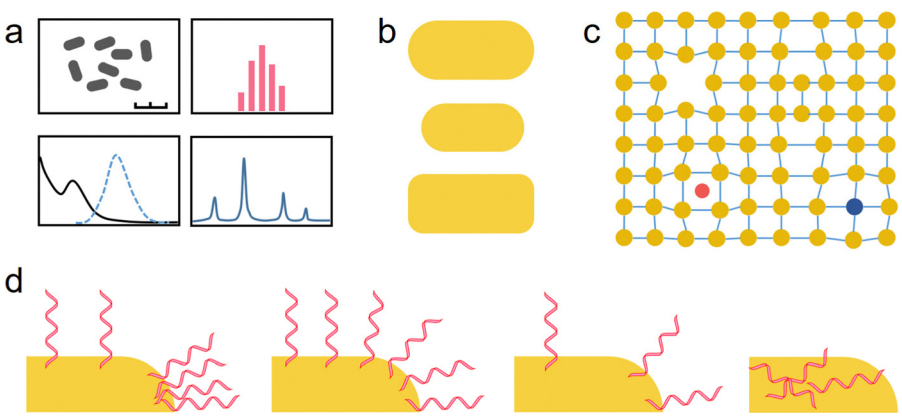

Fig. 12 Limitations of characterization methods for nanostructures. For a batch of crystalline nanostructures that are characterized uniformly by common methods such as TEM imaging, hydrodynamic analysis, photospectrometry test and X-ray diffraction analysis (a), the (b) particle size and shape, (c) species and location of lattice defects, and (d) the density, location and conformation of surface ligands may differ greatly.

more rapidly than surface area with increasing diameter. Therefore, the drug loading efficiency (the drug-to-carrier weight ratio) is greatly improved. Important concerns regarding the use of nanoclusters include the toxicity and the versatility for uploading drugs, since only a small range of molecules can serve as the nanocluster ligands without covalent conjugation.

(iii) Dendrimer nanoparticles may be the closest to clinical applications, as suggested by the number of relevant clinical trials. Dendrimers can be viewed as a special type of polymers but are particulate. The structural defects of dendrimers mainly come from the inter-branch linkage and the failed elongation of some branches due to increased steric hindrance. Like linear polymers that are clinically applicable despite the difficulty in precisely controlling the polymer length, dendrimers may achieve practical applications despite the presence of certain structural defects, because minor defects will influence their property but probably to a less degree than that for crystalline materials whose property heavily depends on particle size and composition.[66,184] For the supramolecular dendrimer nanoparticles, the structural uniformity should be close to that of liposomes (self-assembled from amphiphilic phospholipids) that have achieved clinical applications. The toxicity of dendrimers varies greatly with chemical structure and some cationic ones may cause inflammation;[185] on the other hand, some cationic dendrimers themselves are useful as immunostimulators.[186] The completed and ongoing clinical trials have demonstrated the low toxicity of the tested dendrimers.

(iv) Structural preciseness of carbon nanotubes largely depends on synthesis strategy. Bottom-up routes produce relatively uniform materials compared with the top-down routes, while high structural preciseness is still difficult to achieve using common bottom-up routes, such as solvothermal treatment and chemical vapor deposition. The use of traditional organic synthesis will guarantee a high preciseness. Small-sized GNSs and GNRs can be fully prepared *via* organic synthesis, while for CNTs this is currently impracticable. The use of carbon nanorings as templates directs the growth of CTNs with uniform diameters, although the subsequent epitaxial elongation may increase the structural heterogeneity. Conjugation of hydrophilic groups or oxidation of nanostructures (*e.g.*, producing graphene oxide) is often involved to improve water-solubility but will attenuate the structural preciseness. Therefore, carbon nanostructures may need further development to meet the criterion for bio-applications.

In summary, although other properties, including toxicity and the robustness of performances, are also critical aspects determining whether a material could realize clinical applications, high structural preciseness is considered as a prerequisite. This will help us to understand the material property on a single-particle level, instead of the average property of particles with widely varying structures. Tremendous progress has been made in improving the structural preciseness of nanomaterials in virtue of breakthroughs in synthetic techniques. Currently the above-discussed four types of nanomaterials currently can be molecularly or atomically precise and dendrimer nanoparticles have reached multiple clinical trials, probably due to the high biocompatibility and ease of production. It can be envisioned that with constant progress in the synthesis method, more materials will be prepared precisely and more applications will be realized.

Author contributions

Conceptualization: Jie Wang and Ping Li. Writing original draft: Jie Wang and Ping Li. Review & editing: Chao Wang and Ning Liu. Supervision: Dongming Xing.

Conflicts of interest

There are no conflicts to declare.

Acknowledgements

This work was financially supported by the China Postdoctoral Science Foundation (2021T140355) and the Postdoctoral Innovation Project of Shandong Province (202002025).

Notes and references

1 S. R. D'Mello, C. N. Cruz, M.-L. Chen, M. Kapoor, S. L. Lee and K. M. Tyner, *Nat. Nanotechnol.*, 2017, **12**, 523–529.
2 H. Nsairat, D. Khater, U. Sayed, F. Odeh, A. Al Bawab and W. Alshaer, *Heliyon*, 2022, **8**, e09394.
3 P. Mishra, B. Nayak and R. K. Dey, *Asian J. Pharm. Sci.*, 2016, **11**, 337–348.
4 Z. Tian and W. Yao, *Front. Oncol.*, 2022, **12**, 815900.
5 N. Song, J. Zhang, J. Zhai, J. Hong, C. Yuan and M. Liang, *Acc. Chem. Res.*, 2021, **54**, 3313–3325.
6 P. Dash, A. M. Piras and M. Dash, *J. Controlled Release*, 2020, **327**, 546–570.
7 Y. H. Chung, H. Cai and N. F. Steinmetz, *Adv. Drug Delivery Rev.*, 2020, **156**, 214–235.
8 S. Dordevic, M. M. Gonzalez, I. Conejos-Sanchez, B. Carreira, S. Pozzi, R. C. Acurcio, R. Satchi-Fainaro, H. F. Florindo and M. J. Vicent, *Drug Delivery Transl. Res.*, 2022, **12**, 500–525.
9 C. Egbuna, V. K. Parmar, J. Jeevanandam, S. M. Ezzat, K. C. Patrick-Iwuanyanwu, C. O. Adetunji, J. Khan, E. N. Onyeike, C. Z. Uche, M. Akram, M. S. Ibrahim, N. M. El Mahdy, C. G. Awuchi, K. Saravanan, H. Tijjani, U. E. Odoh, M. Messaoudi, J. C. Ifemeje, M. C. Olisah, N. J. Ezeofor, C. J. Chikwendu and C. G. Ibeabuchi, *J. Toxicol.*, 2021, 9954443.
10 J. M. Rabanel, V. Adibnia, S. F. Tehrani, S. Sanche, P. Hildgen, X. Banquy and C. Ramassamy, *Nanoscale*, 2019, **11**, 383–406.
11 R. Veneziano, T. J. Moyer, M. B. Stone, E. C. Wamhoff, B. J. Read, S. Mukherjee, T. R. Shepherd, J. Das, W. R. Schief, D. J. Irvine and M. Bathe, *Nat. Nanotechnol.*, 2020, **15**, 716–723.

12 H. Lee, A. K. Lytton-Jean, Y. Chen, K. T. Love, A. I. Park, E. D. Karagiannis, A. Sehgal, W. Querbes, C. S. Zurenko, M. Jayaraman, C. G. Peng, K. Charisse, A. Borodovsky, M. Manoharan, J. S. Donahoe, J. Truelove, M. Nahrendorf, R. Langer and D. G. Anderson, *Nat. Nanotechnol.*, 2012, **7**, 389–393.
13 G. Yi, J. Son, J. Yoo, C. Park and H. Koo, *Biomater. Res.*, 2018, **22**, 13.
14 S. B. van der Meer, T. Knuschke, A. Frede, N. Schulze, A. M. Westendorf and M. Epple, *Acta Biomater.*, 2017, **57**, 414–425.
15 Q. Hu, H. Li, L. Wang, H. Gu and C. Fan, *Chem. Rev.*, 2019, **119**, 6459–6506.
16 J. Huang, S. Gambietz and B. Sacca, *Small*, 2022, e2202253, DOI: **10.1002/smll.202202253**.
17 N. C. Seeman, *J. Theor. Biol.*, 1982, **99**, 237–247.
18 N. R. Kallenbach, R.-I. Ma and N. C. Seeman, *Nature*, 1983, **305**, 829–831.
19 T. J. Fu and N. C. Seeman, *Biochemistry*, 1993, **32**, 3211–3220.
20 T. H. Labean, H. Yan, J. Kopatsch, F. Liu, E. Winfree, J. H. Reif and N. C. Seeman, *J. Am. Chem. Soc.*, 2000, **122**, 1848–1860.
21 F. Mathieu, S. Liao, J. Kopatsch, T. Wang, C. Mao and N. C. Seeman, *Nano Lett.*, 2005, **5**, 661–665.
22 J. Zheng, J. J. Birktoft, Y. Chen, T. Wang, R. Sha, P. E. Constantinou, S. L. Ginell, C. Mao and N. C. Seeman, *Nature*, 2009, **461**, 74–77.
23 L. Lin, Y. Pei, Z. Li and D. Luo, *Interdiscip. Med.*, 2022, **1**, e20220008.
24 Y. He, T. Ye, M. Su, C. Zhang, A. E. Ribbe, W. Jiang and C. Mao, *Nature*, 2008, **452**, 198–201.
25 C. Zhang, S. H. Ko, M. Su, Y. Leng, A. E. Ribbe, W. Jiang and C. Mao, *J. Am. Chem. Soc.*, 2009, **131**, 1413–1415.
26 C. Zhang, M. Su, Y. He, X. Zhao, P.-A. Fang, A. E. Ribbe, W. Jiang and C. Mao, *Proc. Natl. Acad. Sci. U. S. A.*, 2008, **105**, 10665–10669.
27 E. Benson, A. Mohammed, J. Gardell, S. Masich, E. Czeizler, P. Orponen and B. Hogberg, *Nature*, 2015, **523**, 441.
28 D. Han, X. Qi, C. Myhrvold, B. Wang, M. Dai, S. Jiang, M. Bates, Y. Liu, B. An, F. Zhang, H. Yan and P. Yin, *Science*, 2017, **358**, eaao2648.
29 P. W. Rothemund, *Nature*, 2006, **440**, 297–302.
30 H. Dietz, S. M. Douglas and W. M. Shih, *Science*, 2009, **325**, 725–730.
31 S. M. Douglas, H. Dietz, T. Liedl, B. Hogberg, F. Graf and W. M. Shih, *Nature*, 2009, **459**, 414–418.
32 D. Han, S. Pal, Y. Liu and H. Yan, *Nat. Nanotechnol.*, 2010, **5**, 712–717.
33 D. Han, S. Pal, J. Nangreave, Z. Deng, Y. Liu and H. Yan, *Science*, 2011, **332**, 342–346.
34 Y. Shang, N. Li, S. Liu, L. Wang, Z. G. Wang, Z. Zhang and B. Ding, *Adv. Mater.*, 2020, **32**, e2000294.
35 P. Kosuri, B. D. Altheimer, M. Dai, P. Yin and X. Zhuang, *Nature*, 2019, **572**, 136–140.
36 D. Jiang, Z. Ge, H. J. Im, C. G. England, D. Ni, J. Hou, L. Zhang, C. J. Kutyreff, Y. Yan, Y. Liu, S. Y. Cho, J. W. Engle, J. Shi, P. Huang, C. Fan, H. Yan and W. Cai, *Nat. Biomed. Eng.*, 2018, **2**, 865–877.
37 B. Wei, M. Dai and P. Yin, *Nature*, 2012, **485**, 623–626.
38 Y. Ke, L. L. Ong, W. M. Shih and P. Yin, *Science*, 2012, **338**, 1177–1183.
39 Y. Ke, L. L. Ong, W. Sun, J. Song, M. Dong, W. M. Shih and P. Yin, *Nat. Chem.*, 2014, **6**, 994–1002.
40 R. D. Barish, R. Schulman, P. W. K. Rothemund and E. Winfree, *Proc. Natl. Acad. Sci. U. S. A.*, 2009, **106**, 6054–6059.
41 W. Liu, H. Zhong, R. Wang and N. C. Seeman, *Angew. Chem., Int. Ed.*, 2011, **50**, 264–267.
42 B. Zhang, T. Tian, D. Xiao, S. Gao, X. Cai and Y. Lin, *Adv. Funct. Mater.*, 2022, **32**, 2109728.
43 S. Li, L. Xu, M. Sun, X. Wu, L. Liu, H. Kuang and C. Xu, *Adv. Mater.*, 2017, **29**, 1606086.
44 Y. He, C. Lv, X. Hou and L. Wu, *Anal. Chim. Acta*, 2020, **1138**, 141–149.
45 J. Yan, J. Chen, N. Zhang, Y. Yang, W. Zhu, L. Li and B. He, *J. Mater. Chem. B*, 2020, **8**, 492–503.
46 T. Wang, Y. Liu, Q. Wu, B. Lou and Z. Liu, *Smart Mater. Med.*, 2022, **3**, 66–84.
47 T. Zhang, T. Tian, R. Zhou, S. Li, W. Ma, Y. Zhang, N. Liu, S. Shi, Q. Li, X. Xie, Y. Ge, M. Liu, Q. Zhang, S. Lin, X. Cai and Y. Lin, *Nat. Protoc.*, 2020, **15**, 2728–2757.
48 W. Zhou, F. Yang, S. Li, R. Yuan and Y. Xiang, *Chem. Sci.*, 2022, **13**, 11132–11139.
49 L. Zhong, S. Cai, Y. Huang, L. Yin, Y. Yang, C. Lu and H. Yang, *Anal. Chem.*, 2018, **90**, 12059–12066.
50 D. Bhatia, S. Arumugam, M. Nasilowski, H. Joshi, C. Wunder, V. Chambon, V. Prakash, C. Grazon, B. Nadal, P. K. Maiti, L. Johannes, B. Dubertret and Y. Krishnan, *Nat. Nanotechnol.*, 2016, **11**, 1112–1119.
51 J. Wang, Q. Li, J. Xue, W. Chen, R. Zhang and D. Xing, *Chem. Eng. J.*, 2021, **410**, 127849.
52 J. Wang, J. Zhou, D. Xu, J. Li and D. Deng, *ACS Appl. Mater. Interfaces*, 2020, **12**, 47197–47207.
53 R. Duangrat, A. Udomprasert and T. Kangsamaksin, *Cancer Sci.*, 2020, **111**, 3164–3173.
54 A. S. Walsh, H. Yin, C. M. Erben, M. J. A. Wood and A. J. Turberfield, *ACS Nano*, 2011, **5**, 5427–5432.
55 Z. Xia, P. Wang, X. Liu, T. Liu, Y. Yan, J. Yan, J. Zhong, G. Sun and D. He, *Biochemistry*, 2016, **55**, 1326–1331.
56 Y. Ma, Z. Wang, Y. Ma, Z. Han, M. Zhang, H. Chen and Y. Gu, *Angew. Chem., Int. Ed.*, 2018, **57**, 5389–5393.
57 S. M. Douglas, I. Bachelet and G. M. Church, *Science*, 2012, **335**, 831–834.
58 X. Liu, F. Zhang, X. Jing, M. Pan, P. Liu, W. Li, B. Zhu, J. Li, H. Chen, L. Wang, J. Lin, Y. Liu, D. Zhao, H. Yan and C. Fan, *Nature*, 2018, **559**, 593–598.
59 T. Tian, Y. Li and Y. Lin, *Bone Res.*, 2022, **10**, 40.
60 A. R. Chandrasekaran, *Nat. Rev. Chem.*, 2021, **5**, 225–239.
61 H. Jun, X. Wang, W. P. Bricker and M. Bathe, *Nat. Commun.*, 2019, **10**, 5419.
62 M. Glaser, S. Deb, F. Seier, A. Agrawal, T. Liedl, S. Douglas, M. K. Gupta and D. M. Smith, *Molecules*, 2021, **26**, 2287.

63 C. Lin, Y. Ke, Z. Li, J. H. Wang, Y. Liu and H. Yan, *Nano Lett.*, 2009, **9**, 433–436.
64 K. R. Kim, H. Y. Kim, Y. D. Lee, J. S. Ha, J. H. Kang, H. Jeong, D. Bang, Y. T. Ko, S. Kim, H. Lee and D. R. Ahn, *J. Controlled Release*, 2016, **243**, 121–131.
65 A. R. Chandrasekaran, J. Vilcapoma, P. Dey, S. W. Wong-Deyrup, B. K. Dey and K. Halvorsen, *J. Am. Chem. Soc.*, 2020, **142**, 6814–6821.
66 D. Deng, Y. Chen, J. Cao, J. Tian, Z. Qian, S. Achilefu and Y. Gu, *Chem. Mater.*, 2012, **24**, 3029–3037.
67 L. Qu and X. Peng, *J. Am. Chem. Soc.*, 2002, **124**, 2049–2055.
68 C. Pu, H. Qin, Y. Gao, J. Zhou, P. Wang and X. Peng, *J. Am. Chem. Soc.*, 2017, **139**, 3302–3311.
69 C. Femoni, M. C. Iapalucci, S. Ruggieri and S. Zacchini, *Acc. Chem. Res.*, 2018, **51**, 2748–2755.
70 A. C. Dharmaratne, T. Krick and A. Dass, *J. Am. Chem. Soc.*, 2009, **131**, 13604–13605.
71 Y. Chen, C. Zeng, D. R. Kauffman and R. Jin, *Nano Lett.*, 2015, **15**, 3603–3609.
72 P. D. Jadzinsky, G. Calero, C. J. Ackerson, D. A. Bushnell and R. D. Kornberg, *Science*, 2007, **318**, 430–433.
73 R. Jin, C. Zeng, M. Zhou and Y. Chen, *Chem. Rev.*, 2016, **116**, 10346–10413.
74 R. Jin, *Nanoscale*, 2010, **2**, 343–362.
75 R. Jin, H. Qian, Z. Wu, Y. Zhu, M. Zhu, A. Mohanty and N. Garg, *J. Phys. Chem. Lett.*, 2010, **1**, 2903–2910.
76 C. Zeng, Y. Chen, A. Das and R. Jin, *J. Phys. Chem. Lett.*, 2015, **6**, 2976–2986.
77 D. C. Gary, M. W. Terban, S. J. L. Billinge and B. M. Cossairt, *Chem. Mater.*, 2015, **27**, 1432–1441.
78 J. Zhang, R. W. Crisp, J. Gao, D. M. Kroupa, M. C. Beard and J. M. Luther, *J. Phys. Chem. Lett.*, 2015, **6**, 1830–1833.
79 H. Liu, Z. Liu and C. Pu, *Nano Res.*, 2022, **15**, 7622–7630.
80 Z. Gan, J. Chen, J. Wang, C. Wang, M. B. Li, C. Yao, S. Zhuang, A. Xu, L. Li and Z. Wu, *Nat. Commun.*, 2017, **8**, 14739.
81 Z. Gan, Y. Lin, L. Luo, G. Han, W. Liu, Z. Liu, C. Yao, L. Weng, L. Liao, J. Chen, X. Liu, Y. Luo, C. Wang, S. Wei and Z. Wu, *Angew. Chem., Int. Ed.*, 2016, **55**, 11567–11571.
82 N. B. Luque and E. Santos, *Langmuir*, 2012, **28**, 11472–11480.
83 A. H. Pakiari and Z. Jamsshidi, *J. Phys. Chem. A*, 2010, **114**, 9212–9221.
84 X. Kang, Y. Li, M. Zhu and R. Jin, *Chem. Soc. Rev.*, 2020, **49**, 6443–6514.
85 Z. Wu, E. Lanni, W. Chen, M. E. Bier, D. Ly and R. Jin, *J. Am. Chem. Soc.*, 2009, **131**, 16672–16674.
86 J. Yang and R. Jin, *ACS Mater. Lett.*, 2019, **1**, 482–489.
87 C. P. Joshi, M. S. Bootharaju, M. J. Alhilaly and O. M. Bakr, *J. Am. Chem. Soc.*, 2015, **137**, 11578–11581.
88 J. Yang and R. Jin, *J. Phys. Chem. C*, 2021, **125**, 2619–2625.
89 T. L. Botha, E. E. Elemike, S. Horn, D. C. Onwudiwe, J. P. Giesy and V. Wepener, *Sci. Rep.*, 2019, **9**, 4169.
90 B. K. Teo and H. Zhang, *Inorg. Chem.*, 1991, **30**, 3115–3116.
91 B. K. Teo, *Inorg. Chem.*, 1994, **33**, 4086–4097.
92 M. S. Bootharaju, C. P. Joshi, M. R. Parida, O. F. Mohammed and O. M. Bakr, *Angew. Chem., Int. Ed.*, 2016, **55**, 922–926.
93 Z. Qin, J. Zhang, C. Wan, S. Liu, H. Abroshan, R. Jin and G. Li, *Nat. Commun.*, 2020, **11**, 6019.
94 T.-A. D. Nguyen, Z. R. Jones, B. R. Goldsmith, W. R. Buratto, G. Wu, S. L. Scott and T. W. Hayton, *J. Am. Chem. Soc.*, 2015, **137**, 13319–13324.
95 J. Ji, G. Wang, T. Wang, X. You and X. Xu, *Nanoscale*, 2014, **6**, 9185–9191.
96 A. Ganguly, I. Chakraborty, T. Udayabhaskararao and T. Pradeep, *J. Nanopart. Res.*, 2013, **15**, 1522.
97 A. N. Beecher, X. Yang, J. H. Palmer, A. L. LaGrassa, P. Juhas, S. J. Billinge and J. S. Owen, *J. Am. Chem. Soc.*, 2014, **136**, 10645–10653.
98 X. D. Zhang, Z. Luo, J. Chen, X. Shen, S. Song, Y. Sun, S. Fan, F. Fan, D. T. Leong and J. Xie, *Adv. Mater.*, 2014, **26**, 4565–4568.
99 S. Kumar and R. Jin, *Nanoscale*, 2012, **4**, 4222–4227.
100 S. R. Bhattacharya, K. Bhattacharya, V. J. Xavier, A. Ziarati, D. Picard and T. Burgi, *ACS Appl. Mater. Interfaces*, 2022, **14**, 29521–29536.
101 L. M. Tvedte and C. J. Ackerson, *J. Phys. Chem. A*, 2014, **118**, 8124–8128.
102 X. D. Zhang, Z. Luo, J. Chen, S. Song, X. Yuan, X. Shen, H. Wang, Y. Sun, K. Gao, L. Zhang, S. Fan, D. T. Leong, M. Guo and J. Xie, *Sci. Rep.*, 2015, **5**, 8669.
103 T. T. Jia, G. Yang, S. J. Mo, Z. Y. Wang, B. J. Li, W. Ma, Y. X. Guo, X. Chen, X. Zhao, J. Q. Liu and S. Q. Zang, *ACS Nano*, 2019, **13**, 8320–8328.
104 H. Kawasaki, S. Kumar, G. Li, C. Zeng, D. R. Kauffman, J. Yoshimoto, Y. Iwasaki and R. Jin, *Chem. Mater.*, 2014, **26**, 2777–2788.
105 Y. Yang, S. Wang, S. Chen, Y. Shen and M. Zhu, *Chem. Commun.*, 2018, **54**, 9222–9225.
106 L. Luo, Z. Liu, X. Du and R. Jin, *J. Am. Chem. Soc.*, 2022, **144**, 19243–19247.
107 W. T. Chang, P. Y. Lee, J. H. Liao, K. K. Chakrahari, S. Kahlal, Y. C. Liu, M. H. Chiang, J. Y. Saillard and C. W. Liu, *Angew. Chem., Int. Ed.*, 2017, **56**, 10178–10182.
108 X. Kang and M. Zhu, *Chem. Soc. Rev.*, 2019, **48**, 2422–2457.
109 S. Li, X. S. Du, B. Li, J. Y. Wang, G. P. Li, G. G. Gao and S. Q. Zang, *J. Am. Chem. Soc.*, 2018, **140**, 594–597.
110 X. Y. Xie, P. Xiao, X. Cao, W. H. Fang, G. Cui and M. Dolg, *Angew. Chem., Int. Ed.*, 2018, **57**, 9965–9969.
111 X. Jiang, X. Wang, C. Yao, S. Zhu, L. Liu, R. Liu and L. Li, *J. Phys. Chem. Lett.*, 2019, **10**, 5237–5243.
112 E. Abbasi, S. F. Aval, A. Akbarzadeh, M. Milani, H. T. Nasrabadi, S. W. Joo, Y. Hanifehpour, K. Nejati-Koshki and R. Pashaei-Asl, *Nanoscale Res. Lett.*, 2014, **9**, 247.
113 P. Patel, V. Patel and P. M. Patel, *J. Indian Chem. Soc.*, 2022, **99**, 100514.
114 J. Bugno, H.-J. Hsu and S. Hong, *J. Drug Targeting*, 2015, **23**, 642–650.
115 R. J. Smith, C. Gorman and S. Menegatti, *J. Polym. Sci.*, 2020, **59**, 10–28.
116 E. N. Augustus, E. T. Allen, A. Nimibofa and W. Donbebe, *Am. J. Polym. Sci.*, 2017, **7**, 8–14.
117 M. A. van Dongen, A. Desai, B. G. Orr, J. R. Baker Jr. and M. M. Holl, *Polymer*, 2013, **54**, 4126–4133.

118 Z. Lyu, L. Ding, A. Y. T. Huang, C. L. Kao and L. Peng, *Mater. Today Chem.*, 2019, **13**, 34–48.
119 M. V. Walter and M. Malkoch, *Chem. Soc. Rev.*, 2012, **41**, 4593–4609.
120 M. Arseneault, C. Wafer and J. F. Morin, *Molecules*, 2015, **20**, 9263–9294.
121 N. Li, T.-H. Tsoi, W.-S. Lo, Y.-J. Gu, H.-Y. Wan and W.-T. Wong, *Polym. Chem.*, 2017, **8**, 6989–6996.
122 C. Chen, P. Posocco, X. Liu, Q. Cheng, E. Laurini, J. Zhou, C. Liu, Y. Wang, J. Tang, V. D. Col, T. Yu, S. Giorgio, M. Fermeglia, F. Qu, Z. Liang, J. J. Rossi, M. Liu, P. Rocchi, S. Pricl and L. Peng, *Small*, 2016, **12**, 3667–3676.
123 P. Garrigue, J. Tang, L. Ding, A. Bouhlel, A. Tintaru, E. Laurini, Y. Huang, Z. Lyu, M. Zhang, S. Fernandez, L. Balasse, W. Lan, E. Mas, D. Marson, Y. Weng, X. Liu, S. Giorgio, J. Iovanna, S. Pricl, B. Guillet and L. Peng, *Proc. Natl. Acad. Sci. U. S. A.*, 2018, **115**, 11454–11459.
124 J. Chen, A. Ellert-Miklaszewska, S. Garofalo, A. K. Dey, J. Tang, Y. Jiang, F. Clement, P. N. Marche, X. Liu, B. Kaminska, A. Santoni, C. Limatola, J. J. Rossi, J. Zhou and L. Peng, *Nat. Protoc.*, 2021, **16**, 327–351.
125 J. Yang, K. Wang, Y. Zheng, Y. Piao, J. Wang, J. Tang, Y. Shen and Z. Zhou, *Angew. Chem., Int. Ed.*, 2022, **61**, e202202128.
126 B. Basly, G. Popa, S. Fleutot, B. P. Pichon, A. Garofalo, C. Ghobril, C. Billotey, A. Berniard, P. Bonazza, H. Martinez, D. Felder-Flesch and S. Begin-Colin, *Dalton Trans.*, 2013, **42**, 2146–2157.
127 V. Brunetti, L. M. Bouchet and M. C. Strumia, *Nanoscale*, 2015, **7**, 3808–3816.
128 J. Nithyanandhan and N. Jayaraman, *J. Org. Chem.*, 2002, **67**, 6282–6285.
129 C. Wu, C. Gao, S. Lu, X. Xu, N. Wen, S. Zhang and M. Liu, *J. Biomed. Mater. Res., Part A*, 2018, **106**, 440–449.
130 E. E. Simanek, *Molecules*, 2021, **26**, 4774.
131 A. M. Caminade and J. P. Majoral, *Molecules*, 2016, **21**, 538.
132 M. Nikzamir, Y. Hanifehpour, A. Akbarzadeh and Y. Panahi, *J. Inorg. Organomet. Polym.*, 2021, **31**, 2246–2261.
133 L. Chen, J. Li, Y. Fan, J. Qiu, L. Cao, R. Laurent, S. Mignani, A. M. Caminade, J. P. Majoral and X. Shi, *Biomacromolecules*, 2020, **21**, 2502–2511.
134 Y. Dong, T. Yu, L. Ding, E. Laurini, Y. Huang, M. Zhang, Y. Weng, S. Lin, P. Chen, D. Marson, Y. Jiang, S. Giorgio, S. Pricl, X. Liu, P. Rocchi and L. Peng, *J. Am. Chem. Soc.*, 2018, **140**, 16264–16274.
135 A. Janaszewska, J. Lazniewska, P. Trzepinski, M. Marcinkowska and B. Klajnert-Maculewicz, *Biomolecules*, 2019, **9**, 330.
136 M. H. Han, J. Chen, J. Wang, S. L. Chen and X. T. Wang, *J. Biomed. Nanotechnol.*, 2010, **6**, 82–92.
137 S. P. Mukherjee, M. Davoren and H. J. Byrne, *Toxicol. In Vitro*, 2010, **24**, 169–177.
138 S. P. Mukherjee, F. M. Lyng, A. Garcia, M. Davoren and H. J. Byrne, *Toxicol. Appl. Pharmacol.*, 2010, **248**, 259–268.
139 M. Ciolkowski, J. F. Petersen, M. Ficker, A. Janaszewska, J. B. Christensen, B. Klajnert and M. Bryszewska, *Nanomedicine*, 2012, **8**, 815–817.
140 K. Zhou, L. H. Nguyen, J. B. Miller, Y. Yan, P. Kos, H. Xiong, L. Li, J. Hao, J. T. Minnig, H. Zhu and D. J. Siegwart, *Proc. Natl. Acad. Sci. U. S. A.*, 2016, **113**, 520–525.
141 D. A. Moreira, S. D. Santos, V. Leiro and A. P. Pego, *Pharmaceutics*, 2023, **15**, 1054.
142 G. Yang, N. Sadeg and H. Belhadj-Tahar, *Drug Des.*, 2017, **6**, 1000144.
143 H. Belhadj-Tahar, A. Chen, Y. Jia, S. Wu, N. Sadeg, H. Zhao, C. Li, G. Gu, Y. Gao and G. Yang, *J. Clin. Oncol.*, 2018, **36**, e15569.
144 H. Belhadj-Tahar, J. Chen, P. Song, J. Zhao, M. Quan, C. Li, X. Gu, G. Yang and Y. Gao, *J. Global Oncol.*, 2019, **5**, 96.
145 L. M. Kaminskas, D. E. V. Pires and D. B. Ascher, *Sci. Rep.*, 2019, **9**, 15465.
146 R. Sharma, A. Sharma, S. P. Kambhampati, R. R. Reddy, Z. Zhang, J. L. Cleland, S. Kannan and R. M. Kannan, *Bioeng. Transl. Med.*, 2018, **3**, 87–101.
147 J. Wang, Y. Zhang, J. Pi, D. Xing and C. Wang, *J. Controlled Release*, 2021, **340**, 149–167.
148 G. Speranza, *Nanomaterials*, 2021, **11**, 967.
149 Y. Segawa, H. Ito and K. Itami, *Nat. Rev. Mater.*, 2016, **1**, 15002.
150 Y.-X. Chen, D. Lu, G.-G. Wang, J. Huangfu, Q.-B. Wu, X.-F. Wang, L.-F. Liu, D.-M. Ye, B. Yan and J. Han, *ACS Sustainable Chem. Eng.*, 2020, **8**, 6657–6666.
151 B. P. Qi, H. Hu, L. Bao, Z. L. Zhang, B. Tang, Y. Peng, B. S. Wang and D. W. Pang, *Nanoscale*, 2015, **7**, 5969–5973.
152 Y. Yan, J. Chen, N. Li, J. Tian, K. Li, J. Jiang, J. Liu, Q. Tian and P. Chen, *ACS Nano*, 2018, **12**, 3523–3532.
153 J. Li, X. Zhang, J. Jiang, Y. Wang, H. Jiang, J. Zhang, X. Nie and B. Liu, *Toxicol. Sci*, 2019, **167**, 269–281.
154 W. Chen, G. Lv, W. Hu, D. Li, S. Chen and Z. Dai, *Nanotechnol. Rev.*, 2018, **7**, 157–185.
155 C. Zhao, X. Song, Y. Liu, Y. Fu, L. Ye, N. Wang, F. Wang, L. Li, M. Mohammadniaei, M. Zhang, Q. Zhang and J. Liu, *J. Nanobiotechnol.*, 2020, **18**, 142.
156 A. Ghaffarkhah, E. Hosseini, M. Kamkar, A. A. Sehat, S. Dordanihaghighi, A. Allahbakhsh, C. van der Kuur and M. Arjmand, *Small*, 2022, **18**, e2102683.
157 S. Chung, R. A. Revia and M. Zhang, *Adv. Mater.*, 2021, **33**, e1904362.
158 N. Abid, A. M. Khan, S. Shujait, K. Chaudhary, M. Ikram, M. Imran, J. Haider, M. Khan, Q. Khan and M. Maqbool, *Adv. Colloid Interface Sci.*, 2022, **300**, 102597.
159 L. Song, J. Shi, J. Lu and C. Lu, *Chem. Sci.*, 2015, **6**, 4846–4850.
160 W. Su, H. Wu, H. Xu, Y. Zhang, Y. Li, X. Li and L. Fan, *Mater. Chem. Front.*, 2020, **4**, 821–836.
161 A. Kalluri, D. Debnath, B. Dharmadhikari and P. Patra, *Method. Enzymol.*, 2018, **609**, 335–354.
162 X. Yan, X. Cui and L.-S. Li, *J. Am. Chem. Soc.*, 2010, **132**, 5944–5945.
163 Q. Li, S. Zhang, L. Dai and L. S. Li, *J. Am. Chem. Soc.*, 2012, **134**, 18932–18935.

164 X. Yan, B. Li, X. Cui, Q. Wei, K. Tajima and L. S. Li, *J. Phys. Chem. Lett.*, 2011, **2**, 1119–1124.
165 G. D. Nguyen, H. Z. Tsai, A. A. Omrani, T. Marangoni, M. Wu, D. J. Rizzo, G. F. Rodgers, R. R. Cloke, R. A. Durr, Y. Sakai, F. Liou, A. S. Aikawa, J. R. Chelikowsky, S. G. Louie, F. R. Fischer and M. F. Crommie, *Nat. Nanotechnol.*, 2017, **12**, 1077–1082.
166 J. R. Sanchez-Valencia, T. Dienel, O. Groning, I. Shorubalko, A. Mueller, M. Jansen, K. Amsharov, P. Ruffieux and R. Fasel, *Nature*, 2014, **512**, 61–64.
167 R. S. K. Houtsma, J. de la Rie and M. Stohr, *Chem. Soc. Rev.*, 2021, **50**, 6541–6568.
168 A. P. Johnson, H. V. Gangadharappa and K. Pramod, *J. Controlled Release*, 2020, **325**, 141–162.
169 L. Chen, Y. Hernandez, X. Feng and K. Mullen, *Angew. Chem., Int. Ed.*, 2012, **51**, 7640–7654.
170 J. Cai, P. Ruffieux, R. Jaafar, M. Bieri, T. Braun, S. Blankenburg, M. Muoth, A. P. Seitsonen, M. Saleh, X. Feng, K. Mullen and R. Fasel, *Nature*, 2010, **466**, 470–473.
171 Y. Choi, S. S. Kim, J. H. Kim, J. Kang, E. Choi, S. E. Choi, J. P. Kim, O. Kwon and D. W. Kim, *ACS Nano*, 2020, **14**, 12195–12202.
172 S. Ligima, *Nature*, 1991, **354**, 56–58.
173 A. Yahyazadeh and B. Khoshandam, *Results Phys.*, 2017, **7**, 3826–3837.
174 F. Yuan, T. Yuan, L. Sui, Z. Wang, Z. Xi, Y. Li, X. Li, L. Fan, Z. Tan, A. Chen, M. Jin and S. Yang, *Nat. Commun.*, 2018, **9**, 2249.
175 Z. Wang, F. Yuan, X. Li, Y. Li, H. Zhong, L. Fan and S. Yang, *Adv. Mater.*, 2017, **29**, 1702910.
176 A. Hussain, Y. Liao, Q. Zhang, E. X. Ding, P. Laiho, S. Ahmad, N. Wei, Y. Tian, H. Jiang and E. I. Kauppinen, *Nanoscale*, 2018, **10**, 9752–9759.
177 P. X. Hou, F. Zhang, L. Zhang, C. Liu and H. M. Cheng, *Adv. Funct. Mater.*, 2021, **32**, 2108541.
178 Y. M. Manawi Ihsanullah, A. Samara, T. Al-Ansari and M. A. Atieh, *Materials*, 2018, **11**, 822.
179 H. Omachi, Y. Segawa and K. Itami, *Acc. Chem. Res.*, 2012, **45**, 1378–1389.
180 H. Omachi, T. Nakayama, E. Takahashi, Y. Segawa and K. Itami, *Nat. Chem.*, 2013, **5**, 572–576.
181 H. Omachi, Y. Segawa and K. Itami, *Org. Lett.*, 2011, **13**, 2480–2483.
182 Z. Zhu, Y. Zhai, Z. Li, P. Zhu, S. Mao, C. Zhu, D. Du, L. A. Belfiore, J. Tang and Y. Lin, *Mater. Today*, 2019, **30**, 52–79.
183 H. Ding, J. S. Wei, P. Zhang, Z. Y. Zhou, Q. Y. Gao and H. M. Xiong, *Small*, 2018, **14**, e1800612.
184 C. Xia, W. Wu, T. Yu, X. Xie, C. van Oversteeg, H. C. Gerritsen and C. de Mello Donega, *ACS Nano*, 2018, **12**, 8350–8361.
185 R. Czarnomysy, A. Bielawska and K. Bielawski, *Int. J. Nanomed.*, 2019, **14**, 7123–7139.
186 A. J. Perise-Barrios, R. Gomez, A. L. Corbi, J. de la Mata, A. Dominguez-Soto and M. A. Munoz-Fernandez, *Nanoscale*, 2015, **7**, 3857–3866.

